学位論文

Local motoneuronal activity regulates the frequency of larval fictive locomotion in a segment-specific manner

運動神経細胞の局所的な活動操作がぜん動運動の頻度変化に与える影響

平成 27 年 12 月博士（科学）申請

東京大学大学院　新領域創成科学研究科

複雑理工学専攻　能瀬研究室

松永　光幸

Abstract

I studied the problem of how central circuits coordinate intersegmental movements, using the peristaltic crawling of *Drosophila* larvae as a model. Larval peristaltic crawling is achieved by propagation of muscle contraction from tail to head, which is in turn generated by sequential activation of motoneurons (MNs) in the corresponding neuromeres (segmental units in the central nervous system). The larval ventral nerve cord (VNC) consists of three thoracic (T1~T3) and eight abdominal neuromeres (A1~A8), each of which contains ~80 MNs. A Previous study in the laboratory characterized the effects of local optical perturbation of MNs and suggested that MNs activity in each neuromere is required for the peristaltic wave to propagate across the segment (Inada et al., 2011). However, since muscle contraction was used to monitor the motor output, how the optical perturbation affects the activity dynamics of the motor circuits was unknown. In this study, I developed an experimental system in which one can study the effects of optical manipulation on MNs activity dynamics, in order to more comprehensively analyze the role of MNs activity in motor wave propagation. In particular, I focused the analysis on the global MNs outputs, namely formation of the forward waves, upon MNs perturbation.

Under a confocal microscopy, I applied photo-stimulation temporally at the motor nerve root, through which all MNs in the hemisegment send axons to the periphery, to inhibit or activate the activity of MNs, while monitoring the motor activity corresponding to forward crawling with an EMCCD camera. I found photo-inhibition of MNs in A5 neuromere dramatically decreases the frequency of the motor waves. I then manipulated the MNs activity in other segments, in order to examine segmental difference. I found photo-inhibition of MNs in middle segments (A4, A5, and A6), but not other segments (A1-A3, A7-A8), decreases the motor frequency. I next studied the effects of local activation and found that photo-activation of MNs in posterior segments A6 and A7 but not in other segments, increases the frequency of forward motor wave. These results indicate that local changes in the activity of MNs affect the activity pattern of the entire motor circuits in a segment specific manner. Furthermore, I found that gap junctions are

involved in this process: the local activity manipulations of MNs did not affect the frequency of motor waves in gap junction mutants. Thus, our data suggest that local MNs activity modulates the frequency of forward motor waves via gap junctions.

Table of contents

Abbreviations

A1-A8: abdominal segment / neuromere 1-8

ATR: all-trans retinal

ChR2: channelrhodopsin2

CNS: central nervous system

CPG: central pattern generator

Fas2: fasciclin2

GFP: green fluorescent protein

GFS: giant fiber system

Glu: glutamate

INs: INs

Inx: Innexin

M1-M21: midbody ganglion 1-21

MN(s): motoneruon(s) / motor neurons(s)

NpHR: Halorhodopsin

PBS: phosphate buffer saline

PCOs: phase-coupled oscillators

PNS: peripheral nervous system

ROI: region of interest

SEG: subesophageal ganglion

ShakB: Shaking-B

SNs: sensory neurons

T1-T3: thoracic segment / neuromere 1-3

UAS: upstream activation sequence

VNC: ventral nerve cord

VGluT: vesicular glutamate transporter

1. Introduction

1-1. Neural circuit and synaptic transmission

Animal locomotion requires sequentially and temporally coordinated activation of neurons in the nervous system, which consists of the central nervous system (CNS) and the peripheral nervous system (PNS) (Fig.1.1). For example, the typical predatory behavior of zebrafish, optomotor response, is achieved by sequential activation of sensory neurons (SNs), interneurons (INs), and motoneurons (MNs) as follows. When presented with a moving stimulus in the visual field, sensory neurons are activated and convey the information to interneurons. Then, interneurons perform complex computation. Finally, the refined activity pattern is transmitted to MNs which contract muscle sequentially, and initiate prey capture behavior (Muto and Kawakami, 2013).

The signal transmission from a neuron to another neuron is accomplished at the synapse. Two major types of neuronal transmission are known: one mediated by electrical synapses and the other by chemical synapses (Fig.1.2). At electrical synapses, ion flows directly through pores (gap junctions) at the connections between neurons, enabling quick communication between neurons. Electrical synapses are composed of two hemi-channels, called connexins in vertebrates, or innexins in invertebrates. When the two hemi-channels that form an electrical synapse have the same voltage-dependencies, the ion pass through these pores bidirectionally, however, when the two hemi-channels have different voltage-dependencies, ion flow can be unidirectional (Phelan, et al., 2008). On the other hand, at chemical synapses, information flow is via the synaptic cleft. Neurotransmitters are released from the presynaptic neuron to the synaptic cleft and are received by receptors on the postsynaptic neurons. Binding of neurotransmitters to the receptors induces various responses, such as influx of ions, depending on the cell type of the postsynaptic neuron.

1-2. Axial locomotion

Locomotion in animal kingdom is diverse (e.g. walking of limbed animals, swimming of fish, and flying of insects). Locomotion can be classified into two types, appendicular locomotion and axial locomotion. In appendicular locomotion, animals push their appendages such as legs, wings and flippers to produce the propulsive force. For example, the grasshopper locust flies in the bush by flapping their wings. In axial locomotion, animals modify their body shape to move. For instance, nematode *C. elegans* moves forward on a substrate by propagating bending waves from anterior-to-posterior along the body (Wen et al., 2012). Swimming of the fish is another example of the axial locomotion. Axial locomotion is used widely in invertebrates and in vertebrates.

1-3. Central pattern generators (CPGs)

Precise patterns of motor activation generates coordinated axial locomotion. Two major hypotheses with respect to the pattern generation have been proposed and extensively studied in various model animals: one is a chain of sequential activity in the central circuits and the other is a chain of sensory reflexes dependent on environmental cues. In 1961, it was shown that even when deprived of all movement-related sensory feedback, the rhythmic and patterned activity resembling flying in locust can be generated (Wilson, 1961). This result that sensory feedback is unnecessary for establishment of a patterned oscillation for flying in locust, established the concept of pattern generating circuits. Later, in 1964, using the swimmeret system of the crayfish as a representative of axial locomotion, Ikeda and Wiersma showed that an isolated CNS still exhibits rhythmic and axially coordinated motor discharges (Fig.1.3). The results indicate that coordinated motor patterns among the segments can be generated by the central circuits. Pattern generating circuits are now called central pattern generators (CPGs) and known to exist in many vertebrates and invertebrates.

1-4. Intersegmental coordination of axial locomotion

In generation of axial locomotion, coordinated and sequential contraction of multiple body parts or segments are required. It is therefore critical to understand how motor activity is coordinated across body segments. The mechanism of intersegmental coordination has been extensively studied with modeling and experiments, especially in lamprey swimming, leech swimming, tadpole swimming and crayfish swimmeret system (Hill et al., 2003, Skinner and Mulloney, 1998). I summarize below some key findings made in previous works in the context of the intersegmental coordination.

There are two model concepts proposed for the coordination: a gradient of excitability and asymmetric coupling between segments (Skinner and Mulloney, 1998). Lamprey swimming is achieved by activating MNs alternately on the left and right side in each of the 100 segments from anterior to posterior. In 1988, phase-coupled oscillators (PCOs) model was developed by Kopell and Ermentrout, in which each oscillator along the spinal cord has the same intrinsic period and is coupled bidirectionally to its nearest neighbors. The PCOs model with an asymmetric circuit, in which the ascending coupling dominates in setting the phase lag, predicts that the entrained frequency reflects the caudal, but not the rostral, oscillator frequency. However, this prediction has proven inconsistent with experiments. Thus the PCOs model was revised, and “synaptic spread” hypothesis has emerged, in which the axons from a segment make the same patterns of synaptic connections in neighboring segments as they do in their own segment, but the strength of distant synapsis is weaker than in their own segment (Williams, 1992). This study demonstrated that asymmetric coupling of oscillators could produce a constant intersegmental phase lag as observed in lamprey swimming. Thus, a link between asymmetric coupling model and the experiments has been made.

On the other hand, in support of a gradient excitability model, Grillner et al. (1993) have proposed a trailing oscillator hypothesis, in which segments are symmetrically coupled but have gradient excitability along the spinal cord segments. The model predicts that phase lag is generated along the body because the leading oscillator has a higher intrinsic frequency. Grillner’s group (Wadden et al., 1997) showed that the

gradient excitability model is also able to produce normal motor pattern. Thus, both asymmetric coupling and gradient excitability models can account for the intersegmental coordination of lamprey swimming.

The models used in the lamprey system were applied with some modifications to other animals including the leech. Leech swimming is achieved by alternate muscle contraction and relaxation that propagate longitudinally from anterior to posterior segments. Unlike in the lamprey, in leech swimming, a gradient of excitability model was not sufficient to generate the stable forward swimming. Unidirectional successive excitation along the body cannot occur because the shortest cycle period is shown to be contained in the middle segments of the VNC. Instead, experimental work has provided evidence that ascending and descending neurons project to different target neurons (Friesen, 1989). A computer model that incorporates these asymmetries, but not the inherent period differences, produced constant phase lag resembling the leech swimming (Cang and Friesen 2002). Thus, it is believed that an asymmetric coupling underlies the coordinated leech swimming.

1-5. *Drosophila* larval crawling as a model

While the modeling and experimental studies in various model animals provided valuable insights on the mechanisms of intersegmental coordination, it was difficult to dissect the function of individual component neurons in the previous experimental system. Furthermore, individual electrophysiological recording does not allow studying the activity dynamics of a population of neurons in the system. As detailed below, recent advent of optogenetics and calcium imaging with genetically-coded calcium indicators, enabled manipulating and visualizing the activity of specific neurons. Accordingly, larval *Drosophila* is emerging as an excellent model system for studies of intersegmental coordination (Kohsaka et al., 2012).

Drosophila larval CNS consists of the brain, subesophageal ganglion (SEG), three thoracic neuromeres (T1, T2, and T3), and eight abdominal neuromeres (A1-A8)

(Fig.1.4C). The segmental identity is conferred by segmentally differential expression of *Homeotic* genes (*Hox* genes). Larval crawling (described below) serves as an excellent model for studies of intersegmental coordination during axial locomotion from the following reasons (Kohsaka et al., 2012). First, the behavior is stereotypic and the underlying circuits are relatively simple. Second, one can use sophisticated genetic techniques to visualize and dissect the function of the component neurons, as I will describe later.

Laval peristaltic crawling is accomplished by the successive bilateral muscle contraction that propagates from tail to head. Muscle contraction in each segment is achieved by sequential activation of motoneurons in the corresponding neuromere in the ventral nerve cord (VNC) (Fox et al., 2006) (Fig.1.4A,B). After completion of one cycle of peristalsis, another wave of muscular contraction immediately follows, which enables rhythmic motion. Observation of the rhythmic motor waves as unidirectional calcium waves by genetically encoded calcium indicators (Kohsaka et al., 2012), enables one to study the effects of various manipulations on the global neural dynamics at spatially and temporally high resolution. The idea that the basic pattern of locomotion is generated in the nerve cord without brain, as in the other animals (e.g. cats, rabbits, the leech, and cockroach [Guertin, 2009, Mullins et al., 2012, Ridgel et al., 2007]) is supported by the results that normal performance of larval locomotion were still observed after removal of the brain and SEG (Berni et al., 2012). Taken together, peristaltic crawling in *Drosophila* larvae is an optimal model to dissect operational mechanisms of the axial locomotion pattern, and intersegmental coordination.

1-6. Regulation of peristaltic crawling by segmental interneurons

Approximately 270 neurons, including ~40 MNs in larval VNC, are contained within each half-segment (or hemi-segment) (Rickert et al., 2011). Since the CNS is packed with these numerous interneurons and their neurites, it had been extremely difficult to identify the neurons included in the system, and to clarify the function of individual component

neurons. Although this had long been a big problem in the field, recent advent of various genetic tools are improving the situation. Here, I introduce two classes of segmental inhibitory interneurons and one class of excitatory interneurons, which have been recently characterized and appear to be involved in the generation of coordinated peristaltic crawling. Inhibitory local interneurons, *period*-positive median segmental interneurons, or PMSIs (Kohsaka et al., 2014), appear to control the locomotion speed by sequentially inhibiting motoneuronal activity in each segment during peristalsis just after motoneuronal activation. Glutamatergic Ventro-Lateral Interneurons (GVLIs: Itakura et al., 2015), another class of inhibitory premotor neurons, like PMSIs, repress motoneuronal activity sequentially during peristalsis, in a later phase than PMSIs. Cholinergic excitatory premotor EVE positive interneurons (Hechsher et al., 2015) are critical for bilateral coordination of the motor outputs (Fox et al., 2006). Although studies on these INs has revealed how MNs activity in each segment is regulated by the action of inhibitory and excitatory inputs, how MN activity is coordinated among multiple segments remains largely unknown.

1-7. Muscle innervation

The information from the upstream INs are relayed to ~40 MNs in each hemi-neuromere in the VNC. Segmental MNs in the VNC send their axons through one of the three branches of the peripheral nerves: intersegmental nerve, segmental nerve, and transverse nerve. In 3rd instar *Drosophila* larvae, two major branches, intersegmental nerve and segmental nerve are bundled together at the nerve root in the VNC. The axons in the bundled nerves again diverge in the body musculature and innervate specific target muscles; intersegmental nerve MNs innervate longitudinal muscles, whereas segmental nerve MNs innervate transverse muscles. The larval neuromuscular synaptic terminals are largely classified into larger type I endings and smaller type II endings. At type I endings, excitatory neurotransmitter, glutamate is released and are further divided to type I big (type-Ib), and type-I small (type-Is). Type-Ib MNs have bigger boutons (about 3-6

μm), project to a single muscle, and are low-threshold, whereas type-1s MNs have smaller boutons (about 2-4 μm), innervate several muscles, and are high-threshold (Choi et al., 2004, Schaefer et al., 2010). It has therefore been proposed that type-Ib and type-Is MNs are specialized for precise and powerful movements, respectively. Type II endings are small (about 1-2 μm) and the terminals are very long. Type II boutons are present on most muscles (Hoang and Chiba, 2001).

1-8. Roles of gap junctions in motor pattern generation

Electrical synaptic transmission among INs and MNs has been observed for a long time in many animal species (e.g. *clione*, *C. elegans*, and leech; Norekian 1999, Kawano et al., 2011, Rodriguez et al. 2012). Recent studies in *C. elegans,* crayfish, and leech begin to elucidate the significance of gap junctions for the dynamics of motor circuits (Kawano et al., 2011, Rela and Szczupak, 2004). For example, *C. elegans* locomotion is controlled by a network of excitatory cholinergic (A- and B-types) and inhibitory GABAergic (D-type) MNs. Power relationship in the activity between the forward circuits coupling to B-type MNs and the backward networks coupling to A-type MNs leads to the choice of forward or backward locomotion (White et al., 1986). Kawano et al. (2011) showed that innexin mutation disrupts gap junctions between A-type MNs and the backward circuits, increases electric activity of the backward circuits and thus results in continuous backward locomotion. In *Drosophila* adults, the giant fiber neuron, a large descending interneuron, mediates the escape behavior by relaying visual stimuli to the MNs that innervate the jump muscles. Phelan et al. (2008) showed that mutations of the *shaking-B* (*shakB*) locus, which lack the function of innexin8 (inx8), a major component of gap junctions in the flies, disrupted electrical coupling between the giant fiber neuron and MNs, and the behavioral response. These results infer that the gap junctions between MNs and the giant fiber interneuron are necessary for the escape behavior. In *Drosophila* larval CNS, it was suggested that MNs couple themselves via electrical synapses. Macleod et al. (2003) injected rhodamine-2 into a motor nerve, and found that the dye diffuses into

MNs not only in the injected neuromere, but also in the neighboring neuromeres. Rhodamine-2 is a small molecule dye that can pass through gap junctions but not the chemical synapses. Thus, MNs in neighboring segments were indicated to be electrically coupled.

1-9. Genetic manipulation and visualization of neural activity

In this section, I summarize key methods used in this study, namely, optogenetics and calcium imaging with genetically-encoded indicators. Details of these molecular tools will also be described in Materials and methods.

1-9-1. GAL4/UAS system

GAL4-UAS expression system enables expression of a transgene reproducibly in specific cells (Brand and Perrimon, 1993) (Fig.1.5). GAL4 is a transcription factor which binds to the UAS sequence and induces transcription of the gene downstream of the UAS sequence. A number of GAL4 lines, which express GAL4 in different subsets of neurons are available. Moreover, various UAS lines that allow expression of reporters and neural probes are available. Thus, by combining various GAL4 lines and UAS lines, reporters and neural probes can be expressed in distinct cells in the animals.

1-9-2. Optogenetics

Optogenetics is a method, which enables activation or inactivation of neurons with spatially restricted illumination with light and utilizes photo-sensitive proteins which allows influx or efflux of ions across the cell membrane. For photo-activation, blue-light sensitive cation channel, Channelrhodopsin2 (ChR2) is most commonly used (Berndt et al., 2011) (Fig.1.6A). Illuminating the neurons expressing ChR2 in their membrane, with ~480 nm blue light, opens the cation channel and allows influx of cation inside of neurons; thus blue light illumination can activate neurons. For photo-inhibition, yellow light sensitive chloride pump, Halorhodopsin3 (NpHR3) is often used (Zhang et al., 2007)

(Fig.1.6B). Illuminating ~560 nm yellow light onto the neurons expressing NpHR3 induces activation of the chloride pumps and influx of chloride ions inside of neurons; thus yellow light illumination can silence neurons. In this way, optogenetics enables manipulation of neurons in a temporally and spatially restricted way with specifically colored light. Since the photo-sensitive channel or pump described above have to couple with all-trans retinal (ATR) to work, larvae have to be fed with ATR for two days before experiments.

1-9-3. Calcium imaging

To visualize global neuronal outputs in the neural circuit, I used calcium imaging.
Neural activation accompanies calcium influx in the neuron. GCaMP protein, which is a GFP (green fluorescent protein) -based calcium indicator, increases its green fluorescent intensity upon biding to calcium (Fig.1.7). Thus, activity can be visualized as elevation of the GCaMP fluorescent intensity, in the neurons which express the probe. Since GCaMP excitation with light (480 nm) does not interfere with NpHR3 excitation light (560 nm), GCaMP imaging can be used for neural silencing experiments. On the other hand, RCaMP is mRuby based calcium indicator which increases red fluorescent intensity upon binding calcium. Since RCaMP excitation light (560 nm) does not interfere with ChR2 excitation light (490 nm), RCaMP imaging can be used with neural activation experiments. I examined simultaneous application of optogenetics and calcium imaging to manipulate motoneuronal activity locally while observing global output of motor circuit.

1-10. Motor perturbation experiments conducted in a previous study

To study the role of MN activity in the motor wave generation, a previous study in our laboratory (Inada et al., 2011) asked if local inhibition of MNs in specific segment(s) using optogenetics affects the propagation of the motor wave. Local and temporal photo-inhibition of MNs was applied to one or a few neuromeres in the VNC, and its effects on

motor wave propagation were examined by observing muscle contraction. They found that local MN inactivation not only induces relaxation of muscles in the corresponding body segments, but also halts the propagation of the peristalsis at the site of manipulation. Furthermore, the peristalsis reinitiated at the site of manipulation when the optogenetic inhibition was turned off. These results suggest that MNs activity in each segment is required for peristaltic wave to propagate across the segment and infer that the information concerning MNs activity is somehow transmitted to other neurons in the central circuits regulating the motor wave. However, the mechanisms mediating this transmission were unknown. Furthermore, since this study used muscle contraction as a measure of motor outputs, it was not possible to study the direct consequence of the local activity manipulation on motor circuit dynamics. The interpretation of the results was also complicated by the fact that the preparation included the body wall muscle and the sensory feedback from muscles.

1-11. Outline of this research

In this study, I extended the study by Inada et al. (2011) by constructing a new experimental system in which one can study the effects of optical manipulation of MNs on global MNs activity dynamics. I also used the isolated CNS without the body wall as a preparation to exclude the involvement of sensory feedback. Furthermore, I explored the molecular mechanisms mediating the transmission of MNs activity to other neurons in the CNS.

In an isolated CNS without the brain, I applied local photo-inhibition to MNs in a single segment with optogenetics. Since I aimed to study the effects of the activity manipulation on global network dynamics, the time length of photo-manipulation was longer than that utilized in the previous study (~30 seconds compared to ~5 seconds in Inada et al., 2011). I found that photo-inhibition of MNs in middle segments (A4, A5 and A6) decreased the motor frequency, whereas the same manipulation in other segments (A1-A3, A7-A8) did not. Conversely, photo-activation of MNs in posterior segments A6

and A7 but not in other segments, increases the frequency of forward motor wave. These results indicate that local activity of MNs is critical for the regulation of global outputs of the entire motor circuits. I also found that gap junctions are involved in this process. Taken together, my data suggest that intersegmental neural connections including gap junctions are critical for the modulation of motor wave. The significance and the underlying possible mechanisms will be discussed.

2. Materials and Methods

2-1. Isolation of nerve cord

For calcium imaging or simultaneous application of calcium imaging and optogenetic stimulation, I used an isolated CNS prepared as described below. Third instar larvae were positioned dorsal-side-up on sylgard-coated petri dishes and pinned through the mouthparts and the posterior abdomen. An incision along the dorsal surface was made with fine scissors and internal organs were removed. The body wall was pinned flat. For preparation of the ventral nerve cord (VNC) with the brain attached, the CNS including subesophageal ganglion (SEG) and the VNC was dissected away from the larval body wall and placed dorsal-side-up on double-sided tape on a glass slide. For preparation of the VNC detached the brain, the two hemispheres were cut away from the VNC with microscissors.. All dissections and experiments were conducted in physiological saline containing 135 mM NaCl, 5 mM KCl, 2 mM $CaCl_2$, 4 mM $MgCl_2$, 5 mM TES, and 36 mM sucrose (Marley et al., 2011).

2-2. Fly stocks

Flies were reared on cornmeal-based food at room temperature 25℃. I used the GAL4/UAS system (Brand and Perrimon, 1993), to drive expression of calcium indicator, GCaMP6m (Chen et al., 2013) or RCaMP (Akerboom et al., 2013) for calcium imaging, to drive expression of yellow light sensitive Cl ion pump NpHR3::mcherry or blue light sensitive cation channel ChR2 (T159C)::YFP for optogenetics, and to drive expression of mCD8::GFP for analysis of anatomy.. *OK6-GAL4* (Aberle et al., 2002) was used for the expression of all MNs except type II MNs (Sanyal, 2009). Glutamatergic-specific-GAL4 driver, *OK371* (Mahr et al., 2006) was used for the expression of all MNs. *C380-GAL4* (Koh et al., 1999), *Cha-GAL80* was used for expression in all MNs (Sanyal, 2009). Fly genome possesses 8 innexin genes that encode protein for gap junction. As a mutant of

innexin8 encoded by *shakB* gene, I used *shakB*^{2} strain. *shaking-B* (*shakB*) gene gives rise to several splicing variants, which translate into at least three distinct proteins: Shaking-B (Neural) (ShakB[N]), Shaking-B(Neural+16) (ShakB[N+16]), and Shaking-B (Lethal) (ShakB[L]). The mutation *shakB*^{2} reduces the expression of *shakB (N)* and *shakB (N+16)* (Phelan et al. 2008) transcript and causes loss of electrical and dye coupling and gap-junction morphology at giant fiber system (GFS) synapses in the adult flies (Phelan et al. 2008).

2-3. Calcium imaging

For calcium imaging experiments without optogentic perturbation, I used genetically encoded calcium indicator GCaMP6m (Chen et al., 2012). GCaMP is a GFP-based calcium indicator which increases fluorescence signal upon binding calcium ions. Third instar larvae expressing GCaMP6m in a subset of neurons were dissected (described above) and placed in physiological saline (described above). I used EMCCD camera (iXon, Andor, U.K.) equipped with a BX61WI Microscope (Olympus, Japan) via C-mount attachment (magnification 1x). Focal plane was set to A5 nerve roots in the VNC. Uniform blue light from a Hg lamp was applied onto the preparation and GCaMP6m signal was detected by EMCCD camera through a standard GFP filter unit (U-MNIBA3, Olympus, Japan). About after 5 minutes from isolation of nerve cord, I started recording neural activities within six ~ seven neuromeres with a water immersion 40x, NA0.8 (Achroplan, Zeiss, Germany) objective lens. 1800 or 2400 or 3000 frames of images were acquired in 10 fps or 5 fps. Thus neural activities were recorded for 3~5 minutes for each preparation. For time-course analysis, I defined a region of interest (ROI) in each nerve root, and plotted the mean fluorescent intensity in the ROIs for each image by image J (National institute of Health, U.S.A.). I detected elevations of fluorescent intensity as neural activations.

2-4. Simultaneous application of calcium imaging and optogenetics

Simultaneous application of photo-inhibition and calcium imaging of MNs, or photo-activation and calcium imaging of MNs were accomplished by the following procedures (Matsunaga et al., 2013) (Fig.2.1).

2-4-1. Photo-inhibition with GCaMP imaging

Photo-stimulation of NpHR3 was accomplished with a stereotyped upright confocal microscopy (FV1000: Olympus). 100mW/mm^2, 559 nm yellow light, which activates NpHR3 was provided by a semi-conductor laser through 559 nm dichroic mirror. Spatial and temporal control of the yellow light was achieved by the galvanometer mirror. As the spot size of laser equipped with a conventional confocal microscope is too small (less than 1μm) to activate group of neurons, laser was defocused to the size of hemi-segment (about 30μm)by incorporating a φ2000μm sized pinhole and an appropriate convex lens along the light pathway. Photo-inhibition was applied for 30 seconds or 60 seconds. A blue light which excites GCaMP was applied to the whole CNS through an additional independent light pathway, and fluorescent signal was detected by an EMCCD camera.

2-4-2. Photo-activation and RCaMP imaging

Simultaneous application of photo-activation and calcium imaging was accomplished with a few modifications from the photo-inhibition and GCaMP imaging system described above. I used light sensitive cation channel ChR2 (T159C)::YFP, and genetically encoded calcium indicator RCaMP. RCaMP is a mRuby-based calcium indicator which increases fluorescence emission upon binding calcium ion. The peak of excitation spectrum of RCaMP is ~575nm, which avoids interference with excitation wavelength of ChR2 (T159C). 6mW/mm^2, 488 nm light which activates ChR2 was provided by argon laser through a 565 nm dichroic mirror. Light from Hg lamp through 545-580 nm filter, which excites RCaMP was illuminated to preparations. RCaMP signal, filtered to ~610 nm was detected by an EMCCD camera.

2-5. Immunohistochemistry

For immunostaining VNC tissues, the larvae were dissected as described above except for the isolation of the CNS, instead, the neural tissues kept attached to the body wall. The samples were fixed in 4% formaldehyde in phosphate buffered saline (PBS) at room temperature for 30 min, washed repeatedly with PBS, placed in PBS with 0.2 %TritonX-100 (PBT), in PBT with normal goat serum, and incubated with primary antibodies overnight at 4℃. After rinses, secondary antibodies were applied. Primary antibodies used in this study are as follows: rabbit anti-GFP (Frontier science, Af2020, 1:1000), mouse anti-Fasciclin2 (Fas2) (DSHB, 1D4, 1:10), rabbit anti-DsRed (Clontech, no.632496, 1:500). Secondary antibodies used are Alexa488-conjugated goat anti-rabbit IgG (Life Technologies, 1:300), Alexa55-conjugated goat anti-mouse IgG (Life Technologies). For imaging and analysis, confocal laser scanning microscope and its software (Fluoview 1000, Olympus, Japan) with a water immersion 20 x (Olympus, Japan), or 60 x objective lens was used.

2-6. Data analysis

Intensity of calcium imaging signal was normalized by the difference between maximum and minimum intensities in all frames, except otherwise mentioned. A calcium wave was defined as the sequential elevation of fluorescent intensity of calcium indicator at least three successive neuromeres.

2-6-1. Frequency of calcium wave

All frames for 30 seconds were used for analysis. $Frequency_{pre,}$ $frequency_{stim}$, and $frequency_{post}$ respectively correspond to frequencies of calcium waves for 30 seconds before onset of photo-stimulation, for 30 seconds after onset of photo-stimulation, and for 30 seconds after termination of photo-stimulation, respectively.

2-6-2. Propagating duration

Propagating duration across segments was defined as time difference between the peaks of motoneuronal fluorescent intensity in distinct segments.

2-6-3. Bilateral intensity difference

The bilateral intensity difference in respective segments during forward calcium wave was averaged from time point of A7 peak to A1 peak. For example, bilateral intensity difference of A4 = $\Sigma |I_{A4left\ k} - I_{A4right\ k}|$ (k = frame number) / number of all frames.

2-6-4. Latency

Latency was defined as the time difference between onset of photo-stimulation and peak of intensity in A2 nerve root of the first calcium wave during photo-stimulation. A2 was selected as a reference of the occurrence of wave, because the elevation of intensity in A2 is stably observable. Note that $latency_{pre}$ was defined as duration between onset of photo-stimulation and the peak of intensity in A2 before the photo-stimulation, whereas $latency_{stim}$ was defined as duration between onset of photo-stimulation and the peak of intensity in A2 during photo-stimulation.

2-7. Statistics

To compare two experimental groups, Student t-test was used. The peak detection of calcium signal was accomplished by Microsoft Excel.

3. Results

3-1. Calcium imaging of MNs activity in isolated CNS with or without brain.

Laval peristaltic crawling is accomplished by successive bilateral muscle contraction which propagates from the tail to head. Muscle contraction in each segment is achieved by activation of MNs in the corresponding neuromere (Fox et al., 2006). Using calcium imaging, the wave-like activity of MNs can be observed in the isolated CNS (Lemon et al., 2015). Although motor waves occur frequently (~1 event/ 1 sec) in intact larvae, motor waves seen in the isolated CNS are much less frequent (~1/ 100sec) (Lemon et al., 2015), which complicates the analysis of the waves. I therefore tested whether removing the brain increases the frequency of peristalsis in dissected larvae and found that it is the case. To further test whether removing the brain also increases the frequency of calcium waves in the isolated CNS, I performed calcium imaging. GCaMP6m was expressed in MNs by *OK6-Gal4* and fluorescence change of GCaMP6m in the nerve root of A1-A8 segments was recorded. Motor activity corresponding to a forward peristalsis (hereafter called a motor wave) was detected as peaks of fluorescent intensity propagating from the posterior to anterior neuromeres (Fig.3.1A-D). I evaluated three parameters of the motor waves in the presence or absence of the brain; frequency, propagating duration, and bilateral coordination. I confirmed that motor waves occurred more frequently in the absence of the brain (without bran: 9.86±0.99 events/min. (n=21), with brain: 0.625±0.08 events/min. (n=8)). The waves also travel faster in the absence of the brain as assessed by the propagating duration of the wave between A7 and A1 (without brain: 1.73±0.246s (n=6), with brain: 12.7s±0.897 (n=8)) (Fig.3.1E,F). In contrast, basic pattern of the waves was not significantly different under the two conditions, including the bilateral symmetry (Fig.3.1G). I therefore used the CNS preparations without the brain in the experiments described below. An independent study also reported recently that forward calcium waves are more frequent in the isolated CNS without the brain (Pulver et al., 2015).

3-2. Photo-inhibition of MNs in an A5 hemi-segment reduces the frequency of the motor wave

Using the preparation described above, I next tried to manipulate MNs activity locally and temporally using optogenetics while observing the motor waves by calcium imaging. In order to simultaneously photo-inhibit and visualize MNs activity, I expressed NpHR3::mcherry and GCaMP6m in MNs. With a confocal microscopy, I applied spatially restricted yellow light for 60 seconds to a motor nerve root in A5 neuromere, while calcium imaging MNs activity by illuminating blue light (Fig.3.2). The photo-stimulation was targeted to the nerve root, since all MNs project to the periphery via the nerve root and thus are likely to be inhibited by the optogenetic manipulation. Light stimulation was confined to one side of the segment (hemi-segment), since it allows calcium imaging of MNs in the other side of the segment. Photo-stimulation was restricted to 30 seconds since too long exposure of the preparations to the light may inactivate NpHR3. Since photo-sensitive channels or pumps require coupling to all-trans retinal (ATR) to function, I used larvae with the same genotype but not fed with ATR as a negative control group.

I found that upon light application, the GCaMP fluorescent intensity decreased in the contralateral side of the manipulated segment A5 (Fig.3.3A,C,C',E). This effect was not seen in the control group (Fig.3.3A,B,D). There are two possible explanations for why photo-inhibition of MNs in one side of the neuromere also decreases the activity (calcium concentration) of MNs in the other hemisegment. One is that since many MNs extend their neurites bilaterally (Kim et al., 2009), they can be inhibited by light application in the other side of the segment. Another possibility is that MNs in two sides of a segment are electrically interconnected since it was inferred that MNs are coupled themselves via gap junctions between neighboring segments (Macleod et al., 2003). I then analyzed the effect of local photo-inhibition on global motor outputs. Surprisingly, the frequency of the motor waves was dramatically decreased by the local stimulation (ATR^+,

pre: 10.4±1.65 events [n=10], stim: 3.6±1.42 events [n=10], post: 10±1.69 events [n=10]; ATR^- control, pre: 10.6±1.56 events [n=7], stim: 10.3±1.48 events [n=7], post: 9.14±1.14 events [n=7]) (Fig.3.3F,G). Furthermore, basal intensity of GCaMP in A3 segment also was reduced upon the A5 photo-inhibition (Fig.3.3H). Thus, local photo-inhibition of MNs in A5 decreased activity of MNs in other segment(s) and the frequency of motor waves. A similar decrease in motor wave frequency was seen when other MN specific Gal4 drivers, *OK371-Gal4* and *C380-Gal4*; *Cha-Gal80,* were used (*OK371-Gal4*, pre: 10.57±0.664 events [n=21], stim: 5.05±0.611 events [n=21] post: 9.43±0.81 events [n=21]; *C380-Gal4*, *Cha-Gal80* driver lines, pre: 8±2 events [n=3], stim: 0.667±0.667 events [n=3], post: 8±2.31 events [n=3]) (Fig.3.3K-P). This excludes the possibility that interneurons contaminated in the MN driver lines were responsible for the phenotype.

A decrease in motor wave frequency could result from either a decrease in the velocity of wave propagation, a decrease in the generation of the wave, or both. In order to examine whether the observed frequency change was linked to the change in the velocity of motor wave, I analyzed propagating duration of motor wave upon the photo-inhibition. I found that the propagating duration across the photo-inhibited segment, was shorter than before photo-inhibited (pre: 0.5 ± 0.062s [n=16], stim: 0.356 ± 0.057) (Fig.3.3I). Thus, the frequency decrease was not due to the change in wave velocity. These data suggest that local inhibition of MNs suppresses the activity of MNs globally and reduces the frequency of the motor wave.

3-3. Photo-inhibition of MNs in middle segments decreased the frequency of the motor wave

I next examined segmental differences in the effects of the photo-inhibition. Photo-inhibition was applied in each of A7 to A1 neuromere (Fig.3.4A). Photo-inhibition of MNs in A4, A5, or A6 reduced the frequency of forward calcium wave, whereas that in A1, A2, A3, or A7 did not (Fig.3.4B,C). Thus, photo-inhibition of MNs in middle segments decreases the wave frequency. The observed segmental difference can not be explained by the difference in the expression level of NpHR3 among segments, since

NpHR3::mcherry expression showed no difference among segments.

I also found that photo-inhibition in A1 increases the frequency of the motor wave. This was shown by examining the latency for wave generation (ATR^+, pre: 7.08±1.01 secs [n=10], stim: 2.86±0.648 secs [n=10]), (ATR^- control, pre: 6.89±1.52 secs [n=9], stim: 5.82±1.27 secs [n=9]) (Fig.3.5A-D). Besides, upon termination of photo-inhibition in A1, the frequency of motor waves was significantly reduced. Since MNs are known to display intense depolarization after inhibition (Inada et al., 2011), post inhibitory rebound of A1 MNs may be involved in this phenomenon. In summary, my results indicate that inhibiting the activity of MNs in a specific segment can either increase or decrease the frequency of the motor wave.

3-4. Photo-activation of MNs in posterior segments increases the frequency of motor wave

Next I examined the effects of local photo-activation of MNs. In order to simultaneously photo-activate and visualize MNs activity, I expressed ChR2 (T159C) and RCaMP in MNs (Fig.3.6A-D). I first photo-activated MNs in A6 hemi-segment by applying blue light locally while illuminating yellow light for calcium imaging using confocal microscopy (Fig.3.6A). As was the case for the photo-inhibition, the local photo-activation affected MN activity in the other side of the segment: RCaMP fluorescent intensity in contra-lateral MNs increased upon photo-activation (Fig.3.7A,C,C',E). No change in the intensity of RCaMP fluorescent intensity was seen in the control group (Fig.3.7A,B,D). I then analyzed the effects of local activation of MNs on global motor activity. Photo-activation of MNs in A6 increased the frequency of forward calcium waves significantly (ATR^+, pre: 8.21±0.793 events [n=19], stim: 12.7±0.994 events [n=19], post: 5.68±1.05 events [n=19]) compared to ATR negative control (pre: 8.57±1.13 events [n=7], stim: 8.29±1.34 events [n=10], post: 7.14±1.34 events [n=7]) (Fig.3.7F,G). Thus, local photo-activation of MNs increases the frequency of forward motor wave. I also observed that RCaMP intensity in the A4 segment increased upon A6 photo-

activation (Fig.3.7H).

I next examined segmental difference in the effects of the photo-activation. Photo-activation was applied to MNs in each of A7 to A1 segment and frequency of the motor waves was analyzed (Fig.3.8A). I found activation of MNs in A6 and A7 increased the frequency of the motor waves (Fig.3.8B,C). In contrast, A2 photo-activation slightly increased the frequency. Photo-activation in A1, A3, A4 and A5 had no significant effect. Thus, hyper-activation of MNs in posterior segment (A6 and A7) but not other segments increases the frequency of the motor wave.

3-5. Effects of local photo-manipulation on motor waves were lost in gap junction mutants

Local photo-inhibition and photo-activation data together indicate that local change in MNs activity affects the activity of distant MNs and the frequency of calcium wave. This suggests that information regarding MN activity is somehow transmitted to distant CNS regions to cause changes in the circuit dynamics. I next tested whether gap junctions are involved in this process, since gap junctions among a group of neurons would enable global neuronal signaling. In *Drosophila* larvae, it had been suggested that MNs are electrically coupled via gap junctions between neighboring segments (Macleod et al., 2003). I used *shakB*^{2} mutants, which lack *Inx8*, a major component of gap junctions in *Drosophila* larval CNS (Stebbings et al., 2002), and tested if the effects of the photo-manipulations are compromised in the mutants. I first applied local photo-inhibition in the gap-junction mutants. As in the control, the photo-inhibition in A5 reduced the fluorescence intensity in contra-lateral MNs. This suggests that the photo-manipulation effectively inhibited the activity of MNs in the manipulated segment in the mutants (Fig.3.9A-C). GCaMP intensity in A3 segment was also reduced upon A5 photo-inhibition as in the control (Fig.3.9E). This suggest that change in MN activity in A5 is normally transmitted to other segment in the mutants, possibly via gap-junctions not including Inx8 or through other mechanisms. However, the photo-inhibition did not

change the frequency of motor waves (*shakB*^{2} mutant, pre: 7.78±1.22 events [n=9], stim: 8.22±1.35 events [n=9] vs control, pre: 10±1.66 events [n=10], stim: 3.6±1.4 [n=10]) (Fig.3.9D). Increase in the wave frequency upon photo-inhibition of A1 also did not occur in *shakB*^{2} mutants (latency in wave generation, pre: 6.96±0.989 sec [n=10], stim: 5.21±1.02 sec [n=10]) (Fig.3.10A-D). Thus, *Inx8* is required for the change in the wave frequency to occur upon the photo-manipulations.

I next examined photo-activation in *shakB*^{2} mutants. Photo-stimulation in A6 raised the fluorescent intensity in contra-lateral MNs, again suggesting that the photo-manipulation was effective in the mutants (Fig.3.11A,B). RCaMP intensity in A4 segment was also increased upon A6 photo-activation as in the control (Fig.3.11D). The increase in the fluorescent intensity was even higher in the mutants than in the control ($p=9.0 \times 10^{-5}$), suggesting the possibility that *shakB*^{2} may suppress hyper-activation caused by the photo-activation (Fig.3.11E). However, change in the frequency of motor wave was not seen in the mutants (*shakB*^{2} mutant, pre: 7.6±1.29 events [n=10], stim: 7.4±1.19 events [n=10] vs control, pre: 8.21±0.79 events [n=7], stim: 12.7±0.99 [n=19]) (Fig.3.11C). Taken together, photo-inhibition and photo-activation data suggest that gap-junctions are involved in the change of wave frequency upon local photo-manipulation of MNs.

4. Discussion

As described in Introduction, a previous study from our laboratory (Inada et al., 2011) studied the effects of local MNs inhibition on larval peristalsis and showed that local MNs activity is critical for motor wave propagation. The results suggested for the presence of synaptic transmission from MNs to other neurons in the CNS that is critical for motor wave propagation. However, since muscle contraction was measured as the motor output, the change in activity dynamics of the motor circuits upon the optical perturbation was unclear. The mechanism of the MNs transmission was also entirely unknown. In addition, involvement of sensory feedback could not be excluded.

In this study, I built a new experimental system, in which one can study the direct causal relationship between the manipulation of MNs activity and change in neural dynamics in the motor circuits, with superior spatial and temporal resolution. Furthermore, I used a preparation in which no sensory feedback is present. Using the new experimental system, I extended the previous study by showing that 1) MNs outputs within the CNS, not mediated by the sensory feedback, is critical for motor wave initiation, 2) there is a segmental difference in the MNs outputs critical for the regulation of the wave, 3) the MNs outputs regulating wave initiation are mediated by gap junctions. Below, I discuss each of these findings.

4-1. Contribution of local motoneuronal activity to generation of motor waves

Here, I showed that manipulation of motoneuronal activity in just one segment robustly affects the output of the entire motor network in *Drosophila* larvae. Photo-inhibition or activation of MNs in a single segment decreased or increased, respectively, the fluorescent intensity in distant neuromeres. Furthermore, photo-inhibition or activation of MNs strongly affected the frequency of motor waves. Thus, change in MNs activity in one segment affects the activity and wave generation of the entire motor system.

It should be noted that in an isolated CNS, peripheral nerves outputting the motor activity and inputting the sensory feedback were severed. The results thus suggest that local MNs activity affects activity of distant MNs through intersegmental neural connection within the CNS, not via sensory feedback of muscle contraction. The identity of the intersegmental connection is currently unknown. It could be direct MN-MN connection since many MNs extend neurites intersegmentally and couple to MNs in the neighboring neuromeres (Kim et al., 2009, Macleold et al., 2003). Alternatively, the intersegmental connection may be with INs such as PMSIs, GVLIs, and EVE positive INs, which have been shown to regulate the activity of MNs (Kohsaka et al., 2014, Itakura et al., 2015, Hechsher et al., 2015).

4-2. Segmental difference in the regulation of wave initiation by MNs activity

In several species, a single ganglion has been shown to be able to produce cyclical motor patterns in isolation, however, intersegmental coordination is necessary to produce a normal motor pattern (locust; Lewis et al., 1973, crayfish; Murchison et al., 1993, leech; Kristan and Calarese, 1976). As I described in the Introduction, two major possible mechanisms for establishment of intersegmental coordination have been proposed; gradient of excitability through segments and asymmetric coupling between segments (Skinner and Mulloney, 1998). These two mechanism of intersegmental coordination have been extensively tested experimentally and by modelling in lamprey, leech, and crayfish (Skinner and Mulloney, 1998, Hill et al., 2003).

In *Drosophila* larvae, Pulver et al. (2015) recently suggested the presence of distributed CPGs across segments. They gradually shortened the chain of neuromeres in the VNC by excision in either a posterior-to-anterior or anterior-to-posterior direction and found that any segment from A2/3 to A8/9 is able to initiate forward waves. These results suggest that the competent CPGs are distributed across segments in *Drosophila* larvae as in the other model animals. In this study, I revealed segmental difference in the

contribution of MNs activity to wave generation and suggested that synaptic connection from MNs to INs may vary among segments (Fig.4.1). The segment specific neural connectivity could be a source of "asymmetric coupling" in this system. Taken together, my study and the study by Pulver et al. (2015) suggest that "asymmetric coupling between segments" could be the mechanism for intersegmental coordination in *Drosophila* larvae.

4-3. Role of gap junctions in intersegmental motor coordination

Recent studies revealed that electrical synapses play important roles in neuronal signal processing. For example, gap junctions are involved in long-lasting synchronized activity in *Clione* and coincidence detection in mammals (Rela and Szczupak, 2004). In *Drosophila* larval CNS, too, it was inferred that MNs in neighboring segments couple themselves via electrical synapses (Macleod, 2003). However, the role of these gap junctions in motor circuits function was unknown.

In this study, I found that increase or decrease in wave frequency upon local photo-manipulation of MNs disappear in $shakB^2$ mutants. The results suggest that gap junctions containing $shakB^2$ are involved in the frequency modulation via MNs. In contrast, the decrease or increase of motoneuronal intensity in distant neuromere upon local manipulation of segmental MNs were not affected in $shakB^2$ mutants. The results suggest that gap junctions containing $shakB^2$ are dispensable for this aspect of motoneuronal communication. Thus, two distinct gap-junction pathways appear to be present in this system: one containing $shakB^2$ mediates MNs outputs critical for the regulation of wave initiation and the other not containing $shakB^2$ is required for coupling among MNs.

In many systems, rectifying electrical synapses are known to be composed by heteromeric assembling of innexins on each side of the apposing neurons (Rela and Szczupak 2004). In *Drosophila*, eight types of innexin genes, innexin 1~8, each of which has several types of isoforms, have been reported (e.g. *shakB [lethal]*, *shakB[neural]*, and *shakB[neural+16]*) (Phelan et al., 2008). This diversity in innexins expression enables

numerous combinations of the channels. In giant fiber system in *Drosophila* adults, Phelan et al. (2008) demonstrated the presence of rectifying electrical synapses between giant fiber neuron and MNs. Coupling of one type of innexin, ShakB (Neural+16) in the giant fiber neuron, and another type of innexin, ShakB (Lethal) in MNs generates rectifying electrical synapses between them. Similarly, in *Drosophila* larval crawling system, heteromeric assembly of ShakB isoforms and other innexins likely constitute rectifying gap junctions.

Based on the assumption that rectifying gap junctions are heterogeneously present in MNs, I discuss below one possible mechanism for the segmental difference I found in the regulation of wave initiation by MNs activity. Let's assume that in middle segments, MNs are connected to the neural circuits regulating the wave frequency via negatively rectifying electrical synapses. This will allow anion flow from MNs to the regulator neurons upon photo-inhibition of MNs, which in turn will result in a decrease in the frequency, while preventing cation flow upon photo-activation of MNs. Similarly, if in posterior segments, MNs are coupled to the regulator neurons via positively rectifying electrical synapses, it is possible to allow cation flow from the MNs to the regulator neurons upon photo-activation of MNs, while preventing anion flow between the neurons upon photo-inhibition of the MNs (Fig.4.2).

4-4. Future prospects

In this study, inhibition of MNs in A4, A5, or A6, but not other segments reduced the frequency of the motor wave. On the other hand, activation of MNs only in A6 or A7 increased the frequency of the wave. Besides, my data suggest that gap-junctions are involved in this process. One interpretation of these results is that segmental MNs couple to putative wave frequency modulating circuits via rectifying electrical synapses in segment specific manner. In order to verify this hypothesis, identification of the component neurons in the wave frequency modulating circuits is necessary. Furthermore, segment specific rectification between these components neurons and segmental MNs

should be shown. These goals may be achieved by observing the change of activity in interneurons upon segmental motor perturbation as follows. By using a binary expression system, genetically encoded calcium indicators can be expressed in all neurons, while optogenetic tools (NpHR3 or ChR2) is expressed specifically in MNs. In such preparations, response of the INs upon the manipulation of MNs in specific segments can be studied. This system may allow identification of INs that are activated or inhibited by the MN activity manipulation and thus are good candidates for the component neurons in the modulating circuits. Once such target INs are identified, one can use the same experimental system to further test whether the information flow is rectified in a segment specific manner. For example, if the target INs that are inhibited by photo-inhibition of MNs in middle segments are identified, one can test whether the inhibition is segment specific. One can also test whether the activity of these neurons are not affected by activation of MNs, as the rectifying hypothesis will predicts. Through these experiments, I anticipate that segment specific rectification and the partners of segmental MNs will be identified.

The experimental system I established in this study can also be applied more generally to the identification and characterization of INs regulating larval locomotion. As described in the Introduction, although several types of INs responsible for the peristaltic crawling have been identified, large population of INs in the motor circuits are still unknown. The experimental system I built enables simultaneous application of restricted photo-manipulation and global imaging of neuronal activity. This will allow one to study the input-output relationship between INs-INs or INs-MNs and thus to identify and functionally characterize novel component INs in the motor circuits.

5. Conclusion

Previously in our laboratory, Inada et al. (2011) first demonstrated the utility of NpHR in *Drosophila* larval crawling as a model. This method enabled analysis of behavioral effect upon optical perturbation on a group of neurons with superb spatial and temporal resolution. However, to analyze the input-output relationship in central circuit, additional modification on this system was necessitated. In this study, using *Drosophila* larval crawling as a model, I first constructed and verified an experimental system, in which one can observe the neural dynamics upon optical manipulation on specific group of neuronal activity.

I investigated how central circuits coordinate locomotor activity through inter-connected segments by observing information flow in the central circuit upon neural perturbation. I found that photo-inhibition of MNs in A4, A5, or A6, but not other segments reduced the frequency of forward calcium wave in isolated CNS. On the other hand, photo-activation of MNs in only A6 or A7 increased the frequency of the wave. Besides, my data suggest that gap-junctions are involved in the MNs-mediated wave regulation. These results revealed a novel mechanism of the regulation of motor circuits in which local MN activity modulates the frequency of motor waves via gap junctions in segment specific manner.

Besides, the experimental system that I constructed here, can be used to study the input-output relationship between INs-MNs or INs-INs by simultaneous application of photo-manipulation of INs and global imaging of motor circuit. I anticipate that, through systematic analysis of functional connectivity in motor circuit, basic mechanism of how central circuits coordinate the movements in animals will be elucidated.

6. References

Aberle H, Haghighi AP, Fetter RD, McCabe BD, Magalhães TR, Goodman CS.
Neuron. 2002 Feb 14;33(4):545-58.
Wishful thinking encodes a BMP type II receptor that regulates synaptic growth in *Drosophila*.

Akerboom J, Carreras Calderón N, Tian L, Wabnig S, Prigge M, Tolö J, Gordus A, Orger MB, Severi KE, Macklin JJ, Patel R, Pulver SR, Wardill TJ, Fischer E, Schüler C, Chen TW, Sarkisyan KS, Marvin JS, Bargmann CI, Kim DS, Kügler S, Lagnado L, Hegemann P, Gottschalk A, Schreiter ER, Looger LL.
Front Mol Neurosci. 2013 Mar 4;6:2.
Genetically encoded calcium indicators for multi-color neural activity imaging and combination with optogenetics.

Berndt A, Schoenenberger P, Mattis J, Tye KM, Deisseroth K, Hegemann P, Oertner TG.
Proc Natl Acad Sci U S A. 2011 May 3;108(18):7595-600.
High-efficiency channelrhodopsins for fast neuronal stimulation at low light levels.

Berni J.
Curr Biol. 2015 May 18;25(10):1319-26.
Genetic dissection of a regionally differentiated network for exploratory behavior in *Drosophila* larvae.

Berni J, Pulver SR, Griffith LC, Bate M.
Curr Biol. 2012 Oct 23;22(20):1861-70.
Autonomous circuitry for substrate exploration in freely moving *Drosophila* larvae.

Brand AH, Perrimon N.
Development. 1993 Jun 118(2):401-15
Targeted gene expression as a means of altering cell fates and generating dominant phenotypes

Cang J, Friesen WO.
J Neurophysiol. 2002 Jun;87(6):2760-9.
Model for intersegmental coordination of leech swimming: central and sensory

mechanisms.

Chen TW, Wardill TJ, Sun Y, Pulver SR, Renninger SL, Baohan A, Schreiter ER, Kerr RA, Orger MB, Jayaraman V, Looger LL, Svoboda K, Kim DS.
Nature. 2013 Jul 18;499(7458):295-300.
Ultrasensitive fluorescent proteins for imaging neuronal activity.

Choi JC, Park D, Griffith LC.
J Neurophysiol. 2004 May;91(5):2353-65. Epub 2003 Dec 24.
Electrophysiological and morphological characterization of identified motor neurons in the *Drosophila* third instar larva central nervous system.

Fox LE, Soll DR, Wu CF.
J Neurosci. 2006 Feb 1;26(5):1486-98.
Coordination and modulation of locomotion pattern generators in *Drosophila* larvae: effects of altered biogenic amine levels by the tyramine beta hydroxlyase mutation.

Friesen WO.
Journal of Comparative Physiology A. 1989 Dec:166(2):205-215
Neuronal control of leech swimming movements II. Motor neuron feedback to oscillator cells 115 and 28.

Grillner S, Matsushima T, Wadden T, Tegnér J, El Manira A, Wallén P.
Seminars in Neuroscience. 1993 Feb 5:1:17-27
The neurophysiological bases of undulatory locomotion in vertebrates.

Guertin PA.
Brain Res Rev. 2009 Dec 11;62(1):45-56.
The mammalian central pattern generator for locomotion.

Heckscher ES, Zarin AA, Faumont S, Clark MQ, Manning L, Fushiki A, Schneider-Mizell CM, Fetter RD, Truman JW, Zwart MF, Landgraf M, Cardona A, Lockery SR, Doe CQ.
Neuron. 2015 Sep 30. pii: S0896-6273(15)00766-7.
Even-Skipped+ Interneurons Are Core Components of a Sensorimotor Circuit that Maintains Left-Right Symmetric Muscle Contraction Amplitude.

Hill AA, Masino MA, Calabrese RL.
J Neurophysiol. 2003 Aug;90(2):531-8.
Intersegmental coordination of rhythmic motor patterns.

Ikeda K, Wiersma CA.
Comp Biochem Physiol. 1964 May;12:107-15.
AUTOGENIC RHYTHMICITY IN THE ABDOMINAL GANGLIA OF THE CRAYFISH: THE CONTROL OF SWIMMERET MOVEMENTS.

Inada K, Kohsaka H, Takasu E, Matsunaga T, Nose A.
PLoS One. 2011;6(12):e29019.
Optical dissection of neural circuits responsible for *Drosophila* larval locomotion with halorhodopsin.

Itakura Y, Kohsaka H, Ohyama T, Zlatic M, Pulver SR, Nose A.
PLoS One. 2015 Sep 3;10(9):e0136660.
Identification of Inhibitory Premotor Interneurons Activated at a Late Phase in a Motor Cycle during *Drosophila* Larval Locomotion.

Kawano T, Po MD, Gao S, Leung G, Ryu WS, Zhen M.
Neuron. 2011 Nov 17;72(4):572-86.
An imbalancing act: gap junctions reduce the backward motor circuit activity to bias *C. elegans* for forward locomotion.

Kim MD, Wen Y, Jan YN.
Dev Biol.2009 Dec 15;336(2):213-21.
Patterning and organization of motor neuron dendrites in the *Drosophila* larva.

Koh YH, Popova E, Thomas U, Griffith LC, Budnik V.
Cell. 1999 Aug 6;98(3):353-63.
Regulation of DLG localization at synapses by CaMKII-dependent phosphorylation.

Kohsaka H, Okusawa S, Itakura Y, Fushiki A, Nose A.
Dev Growth Differ. 2012 Apr;54(3):408-19.
Development of larval motor circuits in *Drosophila*.

Kohsaka H, Takasu E, Morimoto T, Nose A.
Curr Biol. 2014 Nov 17;24(22):2632-42.
A group of segmental premotor interneurons regulates the speed of axial locomotion in *Drosophila* larvae.

Kopell N, Ermentrout GB.
Mathematical Biosciences 1988 July–August 90:1–2: 87–109
Coupled oscillators and the design of central pattern generators.

Kristan WB Jr, Calabrese RL.
J Exp Biol. 1976 Dec;65(3):643-68.
Rhythmic swimming activity in neurones of the isolated nerve cord of the leech.

Lemon WC, Pulver SR, Höckendorf B, McDole K, Branson K, Freeman J, Keller PJ
Nat Commun. 2015 Aug 11;6:7924.
Whole-central nervous system functional imaging in larval *Drosophila*.

Lewis GD, Miller PL, Mills PS.
Journal of Experimental Biology 1973 59: 149-168;
Neuro-Muscular Mechanisms of Abdominal Pumping in the Locust

Macleod GT, Suster ML, Charlton MP, Atwood HL.
J Neurosci Methods. 2003 Aug 15;127(2):167-78.
Single neuron activity in the *Drosophila* larval CNS detected with calcium indicators.

Mahr A, Aberle H.
Gene Expr Patterns. 2006 Mar;6(3):299-309.
The expression pattern of the *Drosophila* vesicular glutamate transporter: a marker protein for MNs and glutamatergic centers in the brain.

Marley R, Baines RA.
Cold Spring Harb Protoc. 2011 Sep 1;2011(9)
Dissection of third-instar *Drosophila* larvae for electrophysiological recording from neurons.

Matsunaga T, Fushiki A, Nose A, Kohsaka H.
J Vis Exp. 2013 Jul 4;(77):e50513. doi: 10.3791/50513.
Optogenetic perturbation of neural activity with laser illumination in semi-intact *Drosophila* larvae in motion.

Murchison D, Chrachri A, Mulloney B.
J Neurophysiol. 1993 Dec;70(6):2620-31.
A separate local pattern-generating circuit controls the movements of each swimmeret in crayfish.

Muto A, Kawakami K.
Front Neural Circuits. 2013 Jun 11;7:110.
Prey capture in zebrafish larvae serves as a model to study cognitive functions.

Norekian TP.
J Neurosci. 1999 Mar 1;19(5):1863-75.
GABAergic excitatory synapses and electrical coupling sustain prolonged discharges in the prey capture neural network of *Clione limacina*.

Phelan P, Goulding LA, Tam JL, Allen MJ, Dawber RJ, Davies JA, Bacon JP.
Curr Biol. 2008 Dec 23;18(24):1955-60.
Molecular mechanism of rectification at identified electrical synapses in the *Drosophila* giant fiber system.

Pulver SR, Bayley TG, Taylor AL, Berni J, Bate M, Hedwig B.
J Neurophysiol. 2015 Aug 26:jn.00731.2015.
Imaging fictive locomotor patterns in larval *Drosophila*

Rela L, Szczupak L.
Mol Neurobiol. 2004 Dec;30(3):341-57.
Gap junctions: their importance for the dynamics of neural circuits.

Rickert C, Kunz T, Harris KL, Whitington PM, Technau GM.
J Neurosci. 2011 Nov 2;31(44):15870-83.
Morphological characterization of the entire interneuron population reveals principles of neuromere organization in the ventral nerve cord of *Drosophila*.

Rodriguez MJ, Alvarez RJ, Szczupak L.
J Neurophysiol. 2012 Apr;107(7):1917-24.
Effect of a nonspiking neuron on motor patterns of the leech.

Sanyal S.
Gene Expr Patterns. 2009 Jun;9(5):371-80.
Genomic mapping and expression patterns of C380, OK6 and D42 enhancer trap lines in the larval nervous system of *Drosophila*.

Schaefer JE, Worrell JW, Levine RB.
J Neurophysiol. 2010 Sep;104(3):1257-66.
Role of intrinsic properties in *Drosophila* MN recruitment during fictive crawling.

Skinner FK, Mulloney B.
Curr Opin Neurobiol. 1998 Dec;8(6):725-32.
Intersegmental coordination in invertebrates and vertebrates.

Stebbings LA, Todman MG, Phillips R, Greer CE, Tam J, Phelan P, Jacobs K, Bacon JP, Davies JA.
Mech Dev. 2002 May;113(2):197-205.
Gap junctions in *Drosophila*: developmental expression of the entire innexin gene family.

Wadden T, Hellgren J, Lansner A, Grillner S.
Biological Cybernetics 1997:76(1):1-9
Intersegmental coordination in the lamprey: Simulations using a network model without segmental boundaries

Wen Q, Po MD, Hulme E, Chen S, Liu X, Kwok SW, Gershow M, Leifer AM, Butler V, Fang-Yen C, Kawano T, Schafer WR, Whitesides G, Wyart M, Chklovskii DB, Zhen M, Samuel AD.
Neuron. 2012 Nov 21;76(4):750-61.
Proprioceptive coupling within motor neurons drives *C. elegans* forward locomotion.

White JG, Southgate E, Thomson JN, Brenner S.
Philos Trans R Soc Lond B Biol Sci. 1986 Nov 12;314(1165):1-340.

The structure of the nervous system of the nematode *Caenorhabditis elegans*.

Williams TL.
Science. 1992 Oct 23;258(5082):662-5.
Phase coupling by synaptic spread in chains of coupled neuronal oscillators.

Wilson DM.
Journal of Experimental Biology 1961 38: 471-490;
The Central Nervous Control of Flight in a Locust

Zhang F, Aravanis AM, Adamantidis A, de Lecea L, Deisseroth K.
Nat Rev Neurosci. 2007 Aug;8(8):577-81.
Circuit-breakers: optical technologies for probing neural signals and systems

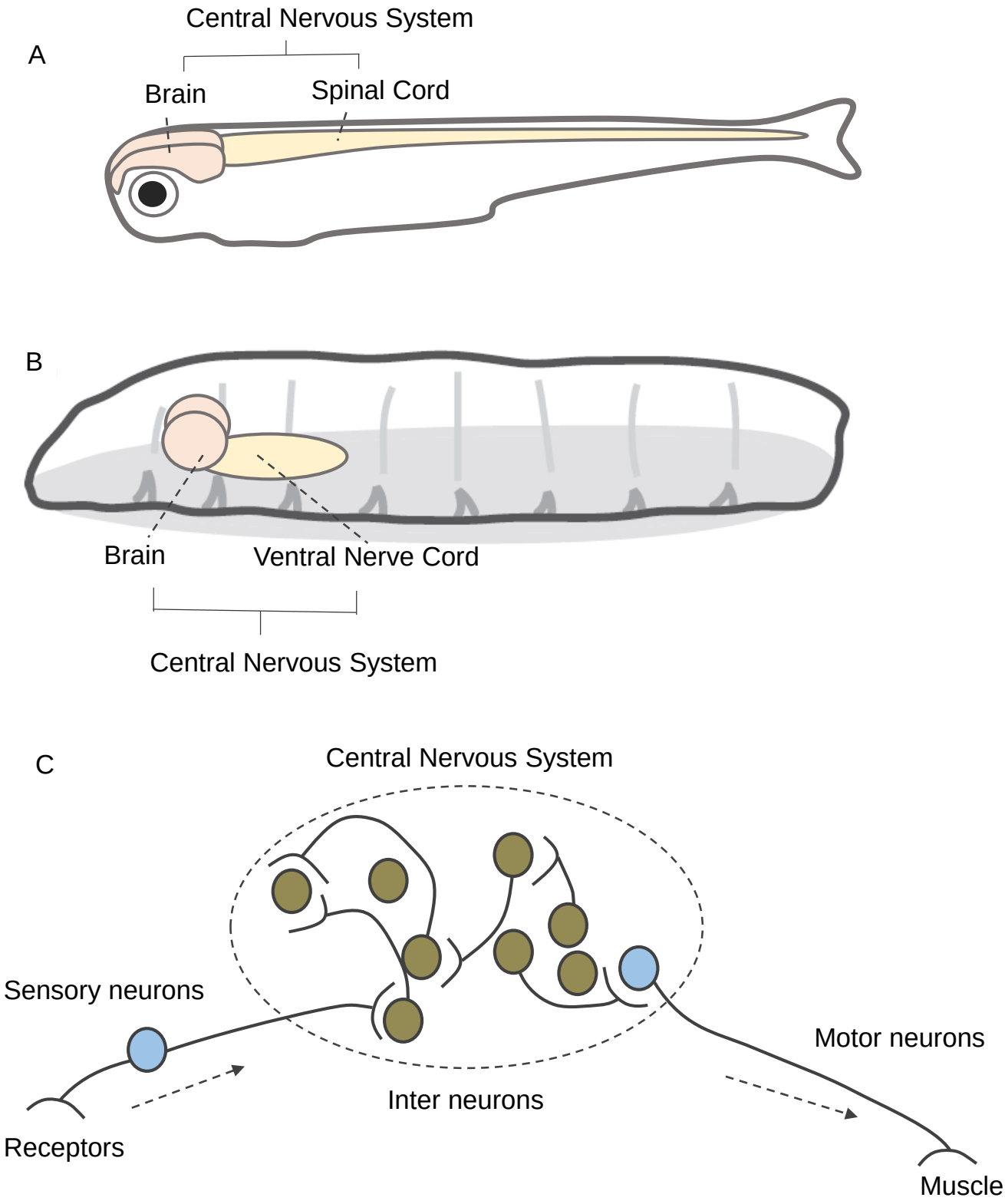

Fig. 1.1 Neural circuits
(A) Central nervous system (CNS) in zebrafish. The CNS consists of the brain and spinal cord. (B) CNS in *Drosophila* larvae. The CNS consists of the brain and ventral nerve cord (VNC). (C) An example of information flow in motor circuit. When presented with external stimuli, sensory neurons are activated and convey the information to interneurons. Then, interneurons perform complex calculation. Finally, the refined activity pattern is transmitted to motoneurons (MNs) which coordinately contract muscles.

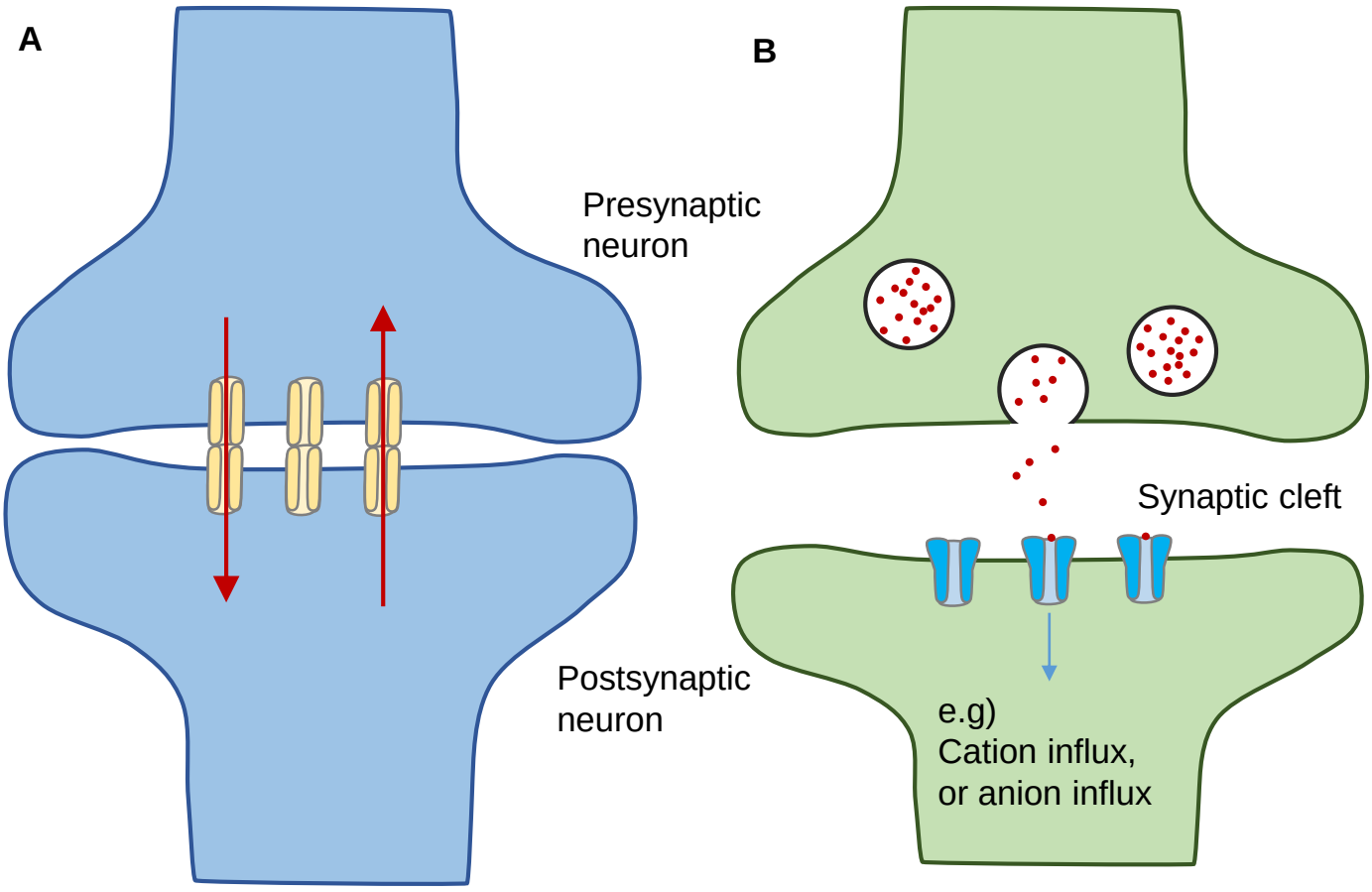

Fig. 1.2 Neural transmission is accomplished at electrical or chemical synapses
(A) At electrical synapses, ions flow directly through pores at connections between the neurons. Thus the communication between the neurons is accomplished quickly. (B) At chemical synapses, information flow takes place at the synaptic cleft. Neurotransmitters are released from the presynaptic neuron to the synaptic cleft and are received by receptors at the postsynaptic neurons.

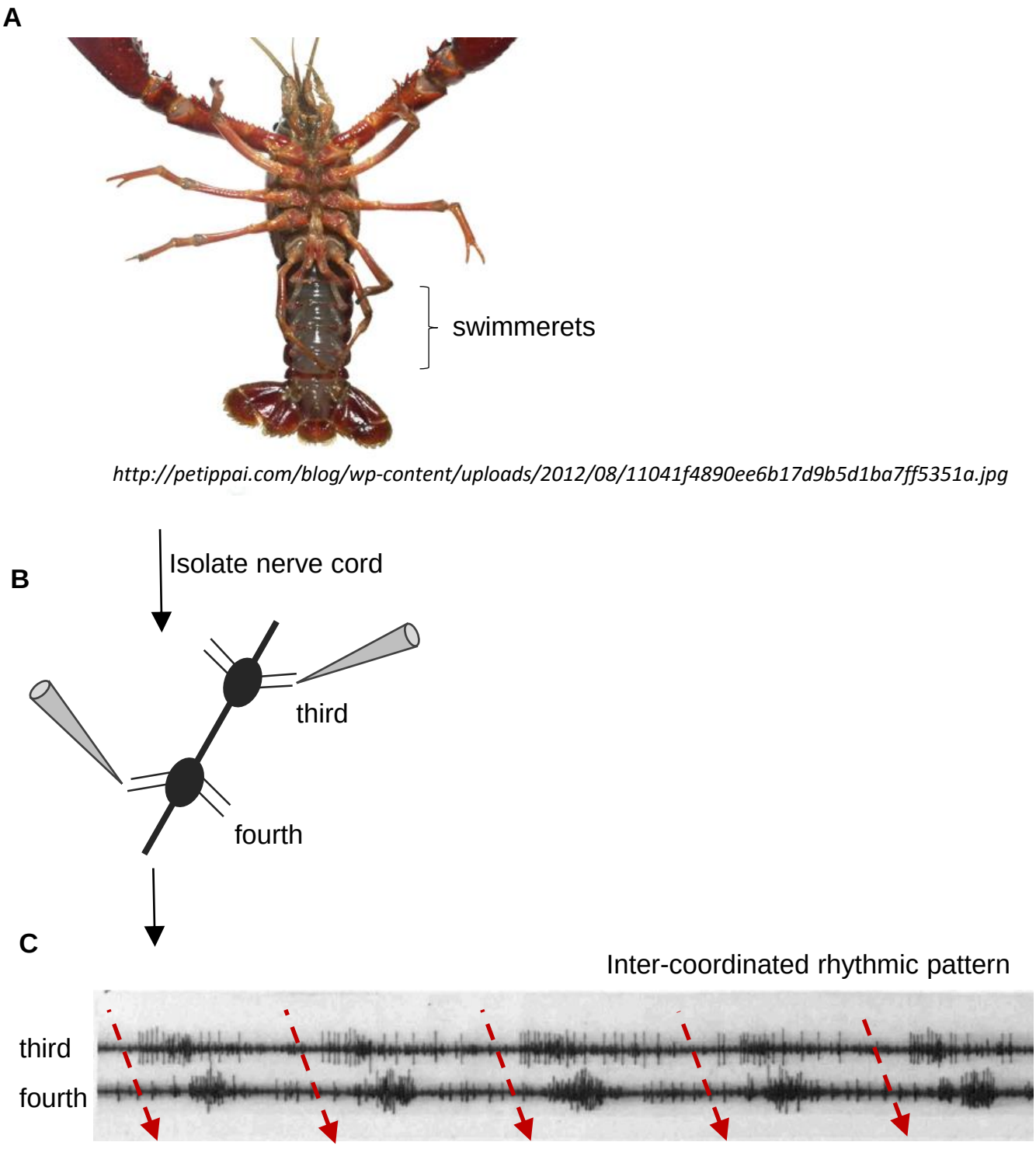

Fig. 1.3 Patterned rhythmic activity is generated by central pattern generators (CPGs) in CNS.
(A) Crayfish. (B) A schematic of the Isolated nerve cord of the crayfish. (C) Recording from the third ganglion (upper trace), and from the fourth ganglion (lower trace). Inter-segmental rhythm was propagated from anterior-to-posterior. The activity in the two segments are tightly linked.

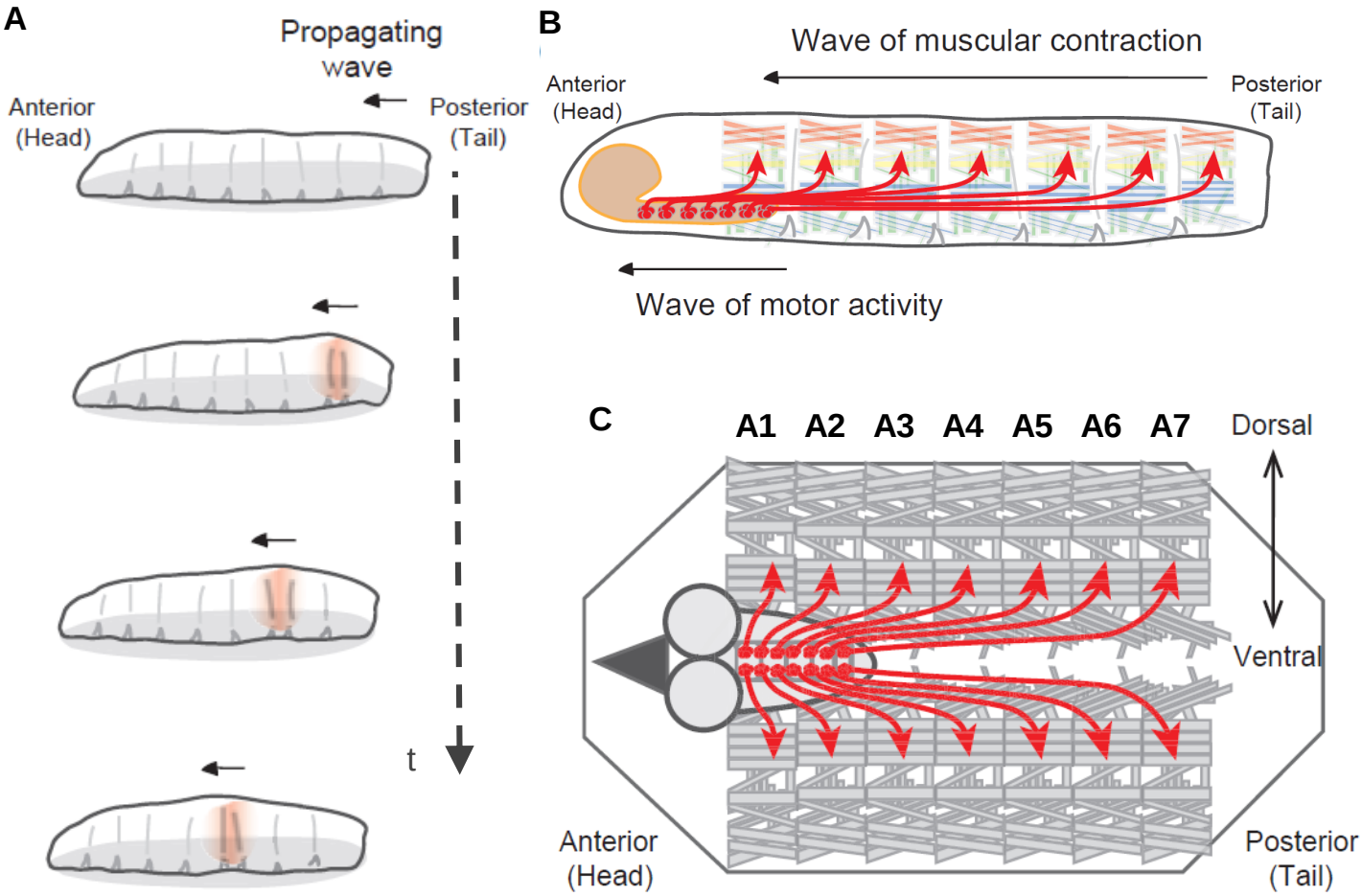

Fig. 1.4 Larval peristaltic crawling and the innervation of muscle by the corresponding MNs

(A) The larval peristaltic crawling is accomplished by the successive bilateral muscle contraction which propagates from the tail to the head. (B) Muscle contraction in each segment is achieved by the sequential activation of MNs in corresponding neuromere in VNC. (C) The correspondence of the muscle and MNs in each segment in dissected larvae. Each body segment and corresponding neuormere in abdomen are named A1 to A7.

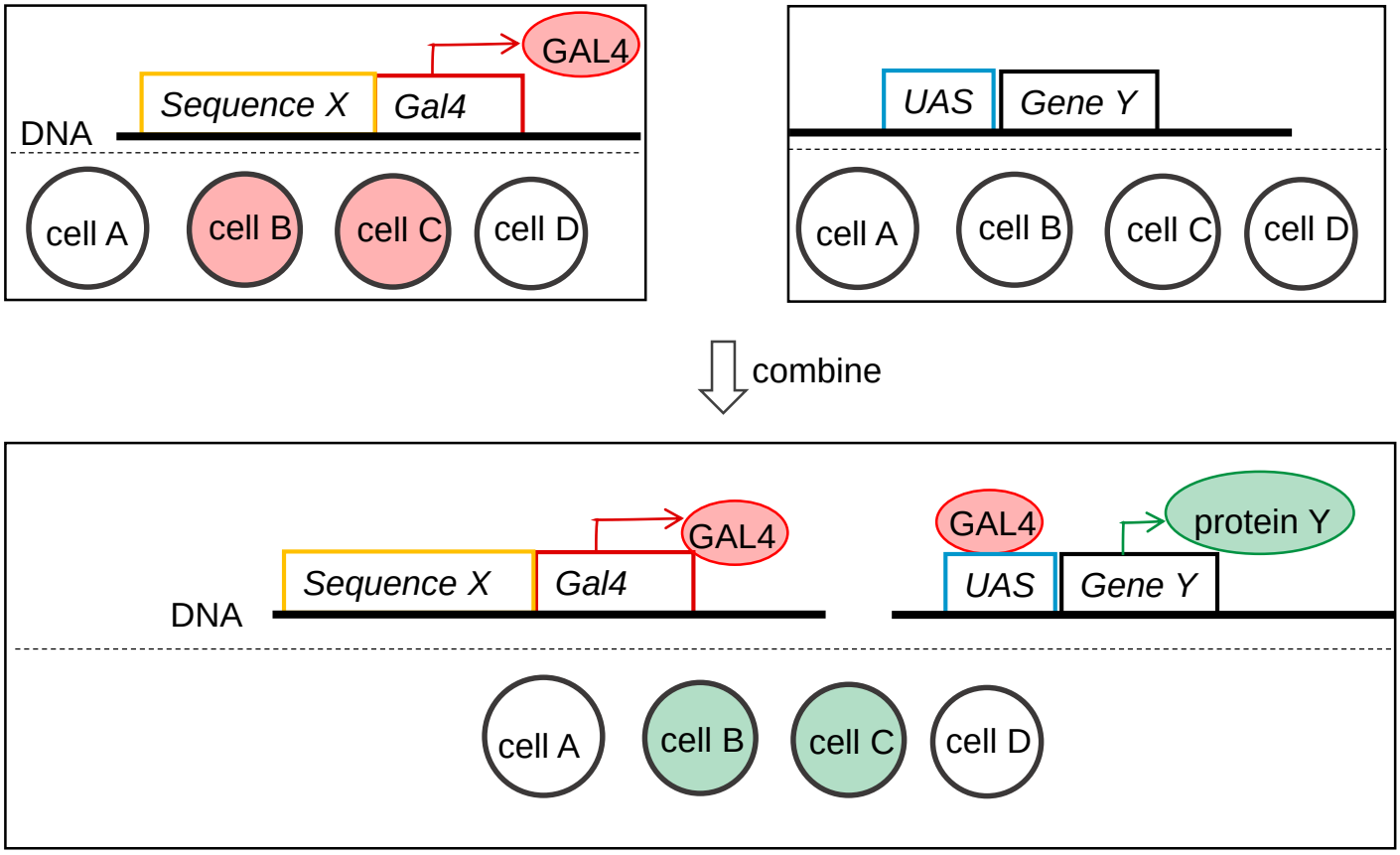

Fig. 1.5 cell specific gene expression by GAL4/UAS system
Gal4 gene is flanked by a particular regulatory sequence, here shown as "*Sequence X*". In the neurons expressing transcription factors which induce gene expression downstream of *Sequence X*, GAL4 protein is produced. *Gene Y*, downstream of *UAS* sequence is expressed only in the presence of GAL4 protein. Thus, in animals possessing both *Gal4* and *UAS* transgenes, protein Y is expressed specifically in the cells marked by *Sequence X*.

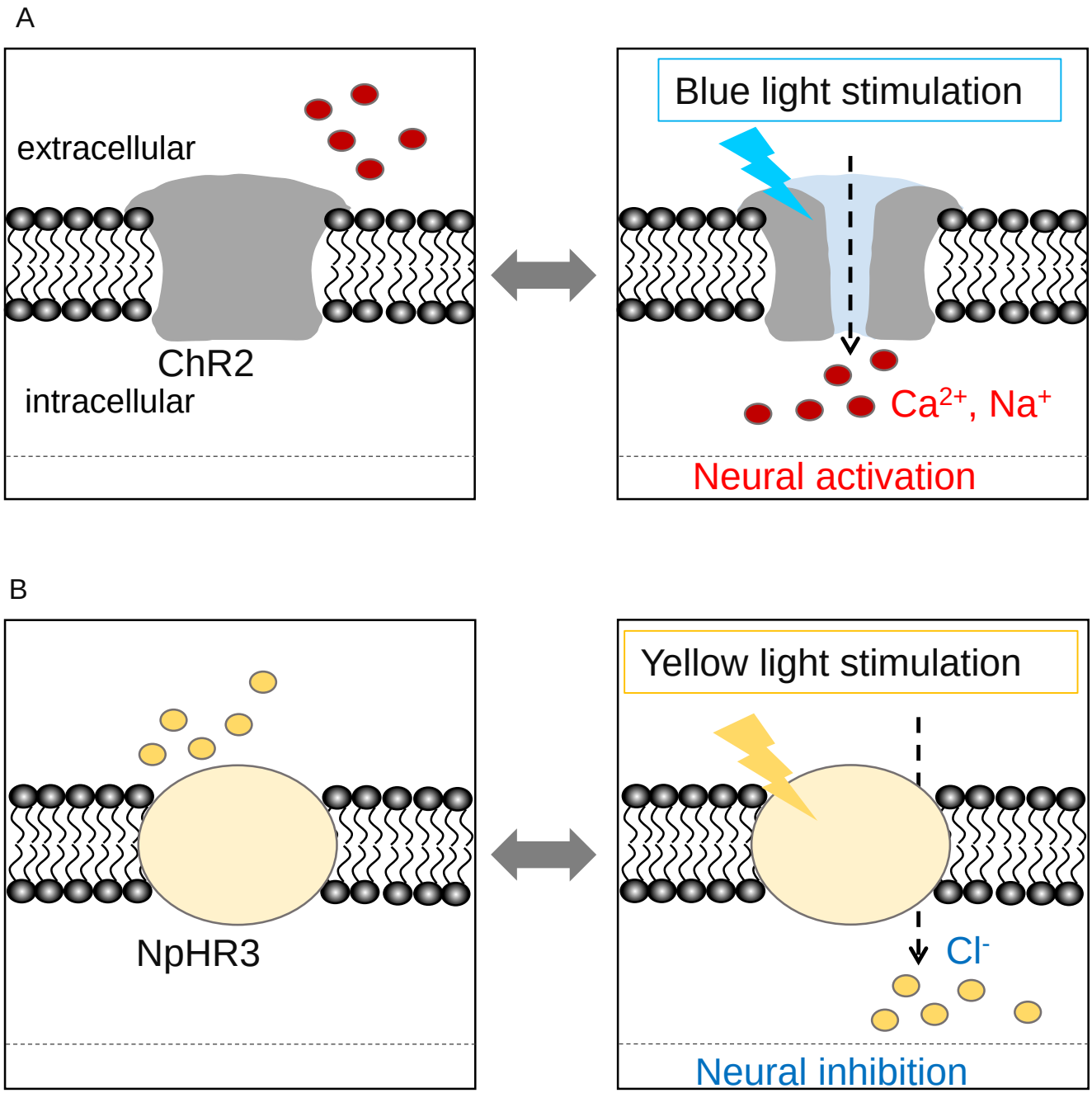

Fig. 1.6 Optogenetic methods to photo-activate or to photo-inhibit neural activity

(A) The neurons expressing cation channel Channelrhodopsin2 (ChR2) are activated by blue light illumination. (B) The neurons expressing yellow light sensitive chloride pump Halorhodpsin3 (NpHR3) are inactivated by yellow light illumination.

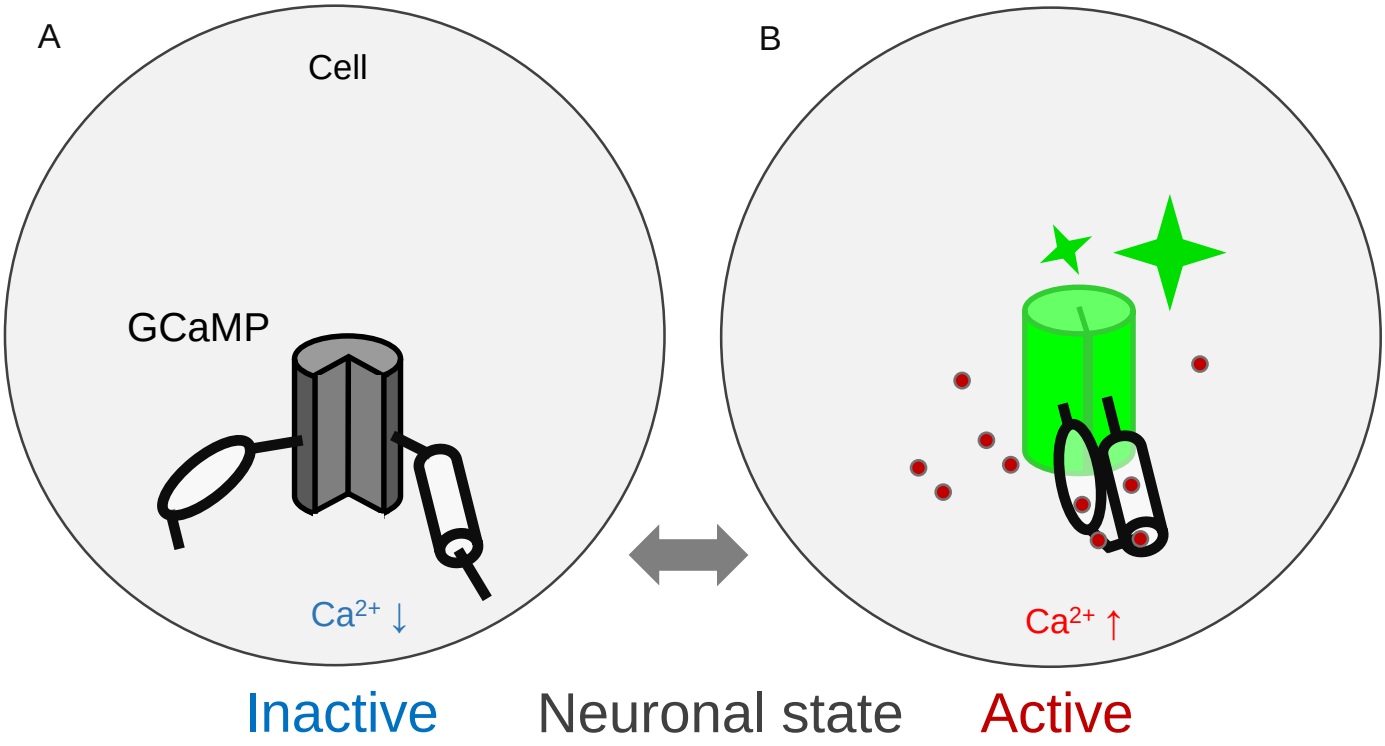

Fig. 1.7 Fluorescent intensity of GCaMP rise under high [Ca].
GCaMP, which is GFP-based calcium indicator, increase a green fluorescent intensity upon binding calcium. Since neuronal activity accompanies calcium influx, neural activity can be visualized as elevation of GCaMP fluorescent intensity. (A) When intracellular [Ca^{2+}] is low (thus neuron inactive), GCaMP fluorescent intensity is low. (B) When intracellular [Ca^{2+}] is high (thus neuron active), GCaMP fluorescent intensity is intensive.

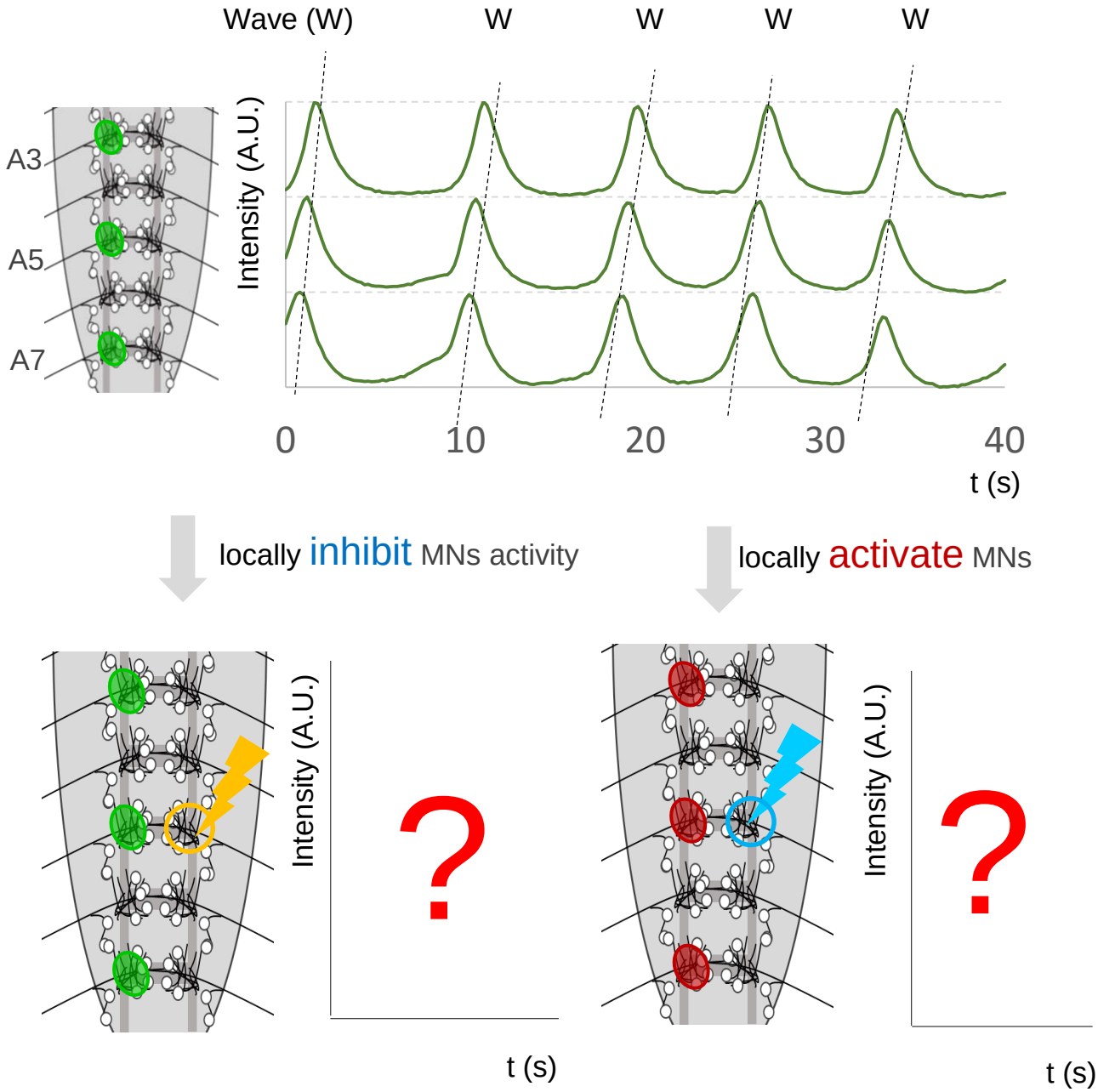

Fig. 2.1 Schematic of local photo-inhibition and photo-activation of MNs in segmental specific manner with calcium imaging
Photo-inhibition (lower left) or activation (lower right) of the motoneuronal activity in segment specific manner was applied while motoneuronal activity was being imaged in isolated nerve cord. The effect upon photo-inhibition (lower left) or activation (lower right) of MNs in segment specific manner was analyzed.

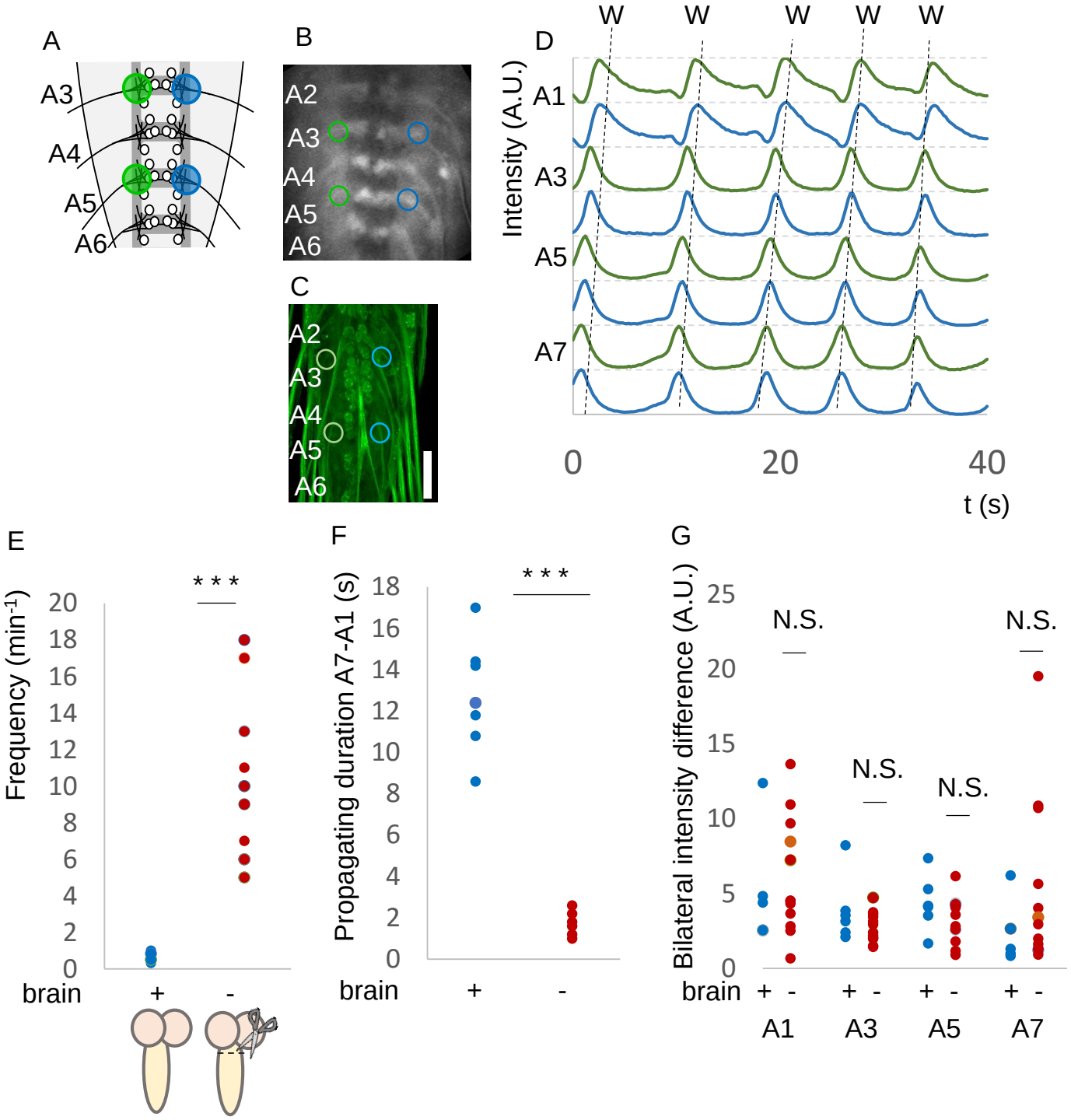

Fig. 3.1 Quantification of forward calcium wave under with or without brain
(A) Schematic of calcium imaging of MNs in isolated VNC (A3-A6). Each circle indicates a region of interest. (B) Single frame of GCaMP imaging. Fluorescent intensity in MNs are visualized by expressing GCaMP6m in *OK6-Gal4* neurons. Each circle indicates a region of interest. (C) mCD8::GFP was expressed in *OK6-Gal4* neurons. Each circle indicates a region of interest. Scale bar, 50 μm. (D) Representative plots of calcium imaging of MNs activity at nerve roots of each neuromere. GCaMP signals in A1, A3, A5, A7 were plot bilaterally. Green and blue lines correspond to GCaMP signals in left and right nerve root, respectively. (E) Frequency of forward calcium wave in the VNC with brain, and without brain. (F) Propagating duration (A7-A1) of forward calcium wave in the VNC with brain and without brain. (G) Bilateral intensity difference of calcium wave in A1, A3, A5, and A7. * * * P<0.001

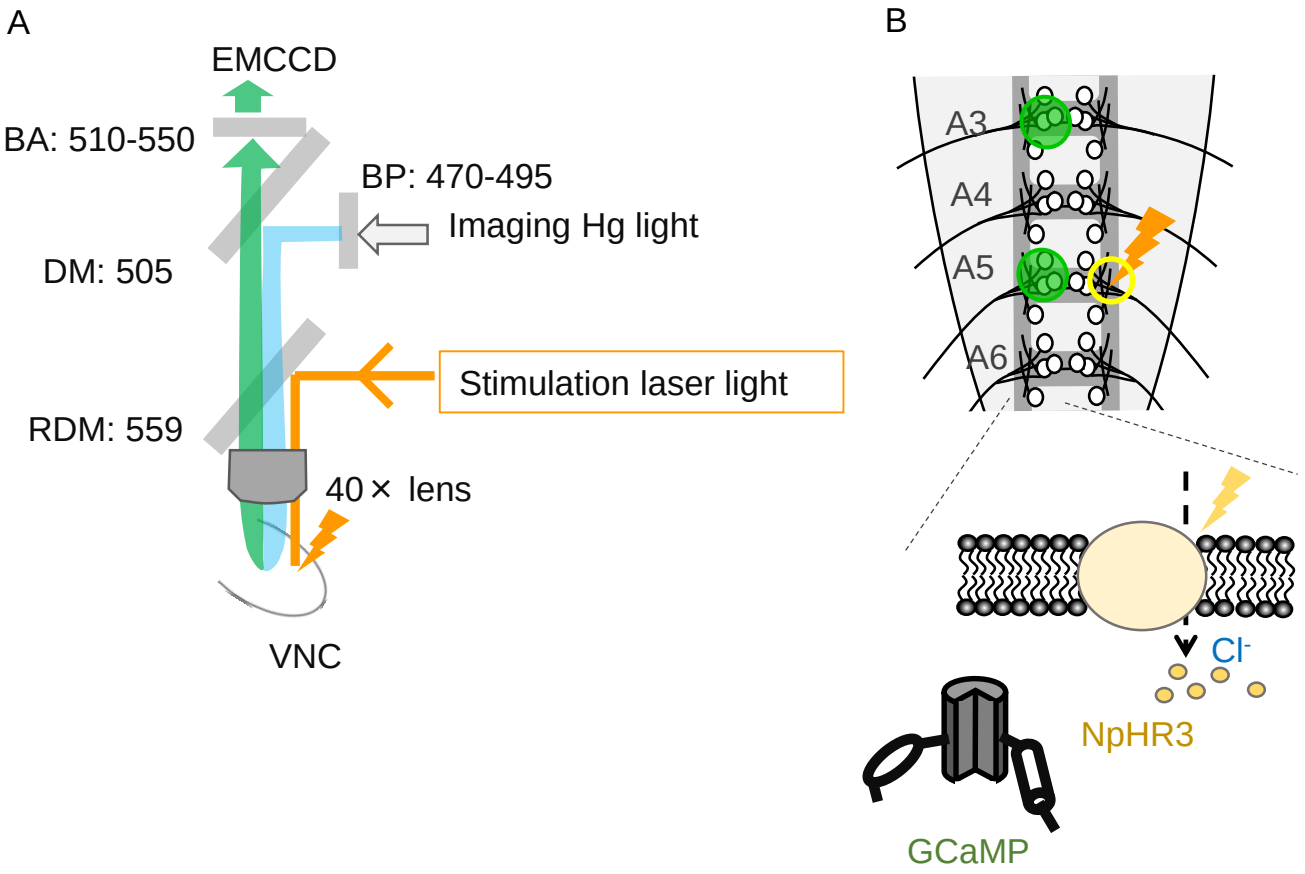

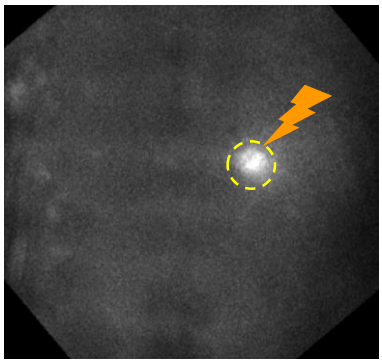

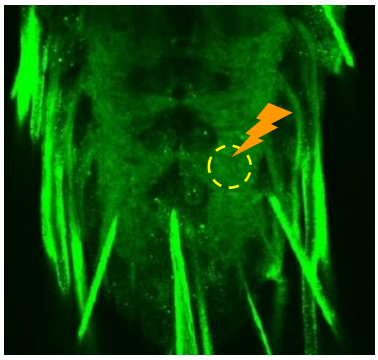

Fig. 3.2 Experimental system of simultaneous application of local photo-inhibition and calcium imaging.
(A) Schematic of simultaneous application of photo-inhibition and GCaMP imaging. BA; barrier filter, DM; dichroic mirror, RDM; reverse dichroic mirror, BP; band pass filter. (B) Schematic of site of optogenetic manipulation. Photo-inhibition of MNs activity was applied in yellow circle. Green circles indicate a region of interest. (C) Single frame of GCaMP imaging of *OK6-Gal4* neurons when photo-inhibition was applied in expression of GCaMP6m and NpHR3::mcherry in *OK6-Gal4* neurons. (D) Expression pattern of the NpHR3::mcherry in *OK6-Gal4* line was assessed. Green represents mcherry expression. Photo-inhibition of MNs activity was applied in yellow circle.

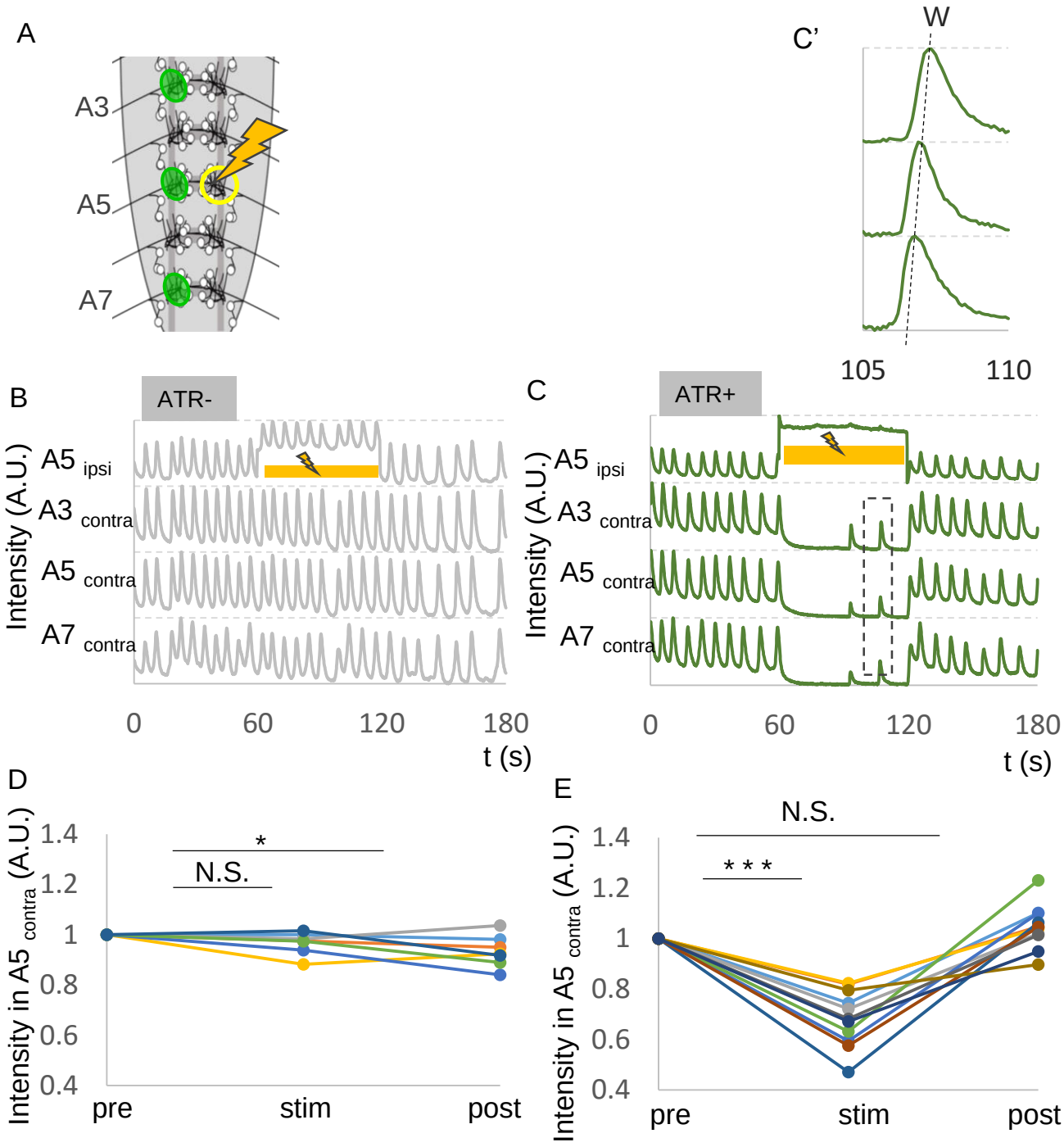

Fig. 3.3 Segment specific photo-inhibition of MNs in A5 decreased frequency of forward calcium wave dramatically.

A) Schematic of photo-inhibition application in A5 hemi-segment specifically. (B, C) Representative results of GCaMP imaging with optogenetic inhibition by NpHR3 in MNs are shown in expression of GCaMP6m and NpHR3::mcherry in *OK6-Gal4* neurons in (B) ATR- control, (C) ATR+ experimental group. Yellow bar indicates yellow light stimulation. Fluorescence intensity in A3 contra, A5 ipsi and contra, and A7 contra nerve root each was plotted. C') Zoomed up image in (C) from 105 seconds to 110 seconds. Broken black bar indicates a forward calcium wave. (D, E) Intensity in A5 contra, before, during, and after A5 photo-stimulation was applied to (D) ATR- control (E) ATR+ experimental group. *P<0.05, ***P<0.001

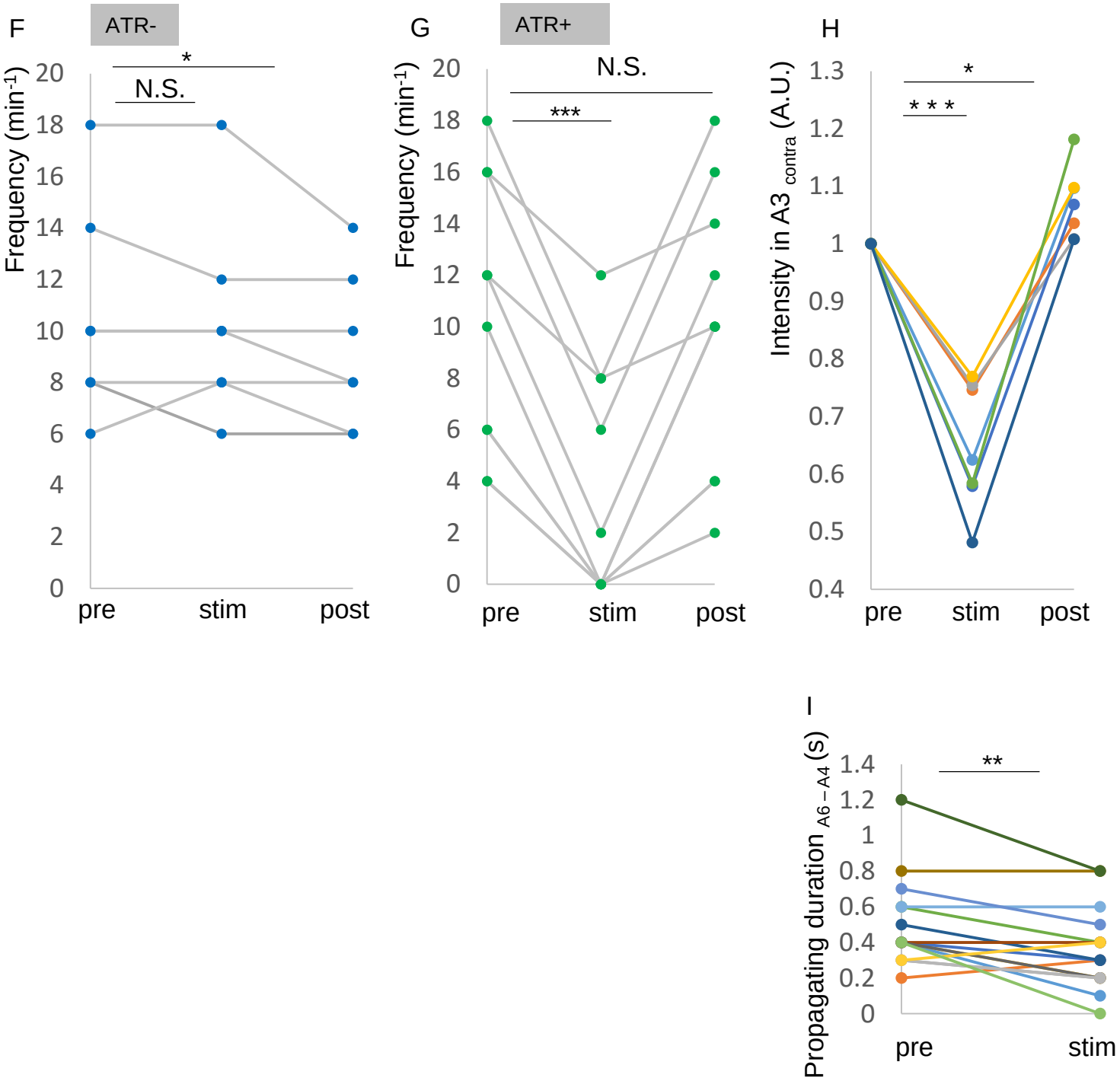

Fig. 3.3 Segment specific photo-inhibition of MNs in A5 decreased frequency of forward calcium wave dramatically.
(F, G) Frequency of forward calcium wave, before, during, and after A5 photo-stimulation was applied to (F) ATR- control, (G) ATR+ experimental group. (H) Intensity in A3 ipsi, before, during, and after A5 photo-stimulation was applied. (I) The propagating duration between A6-A4, before and during A5 photo-stimulation was applied. *P<0.05, ***P<0.001.

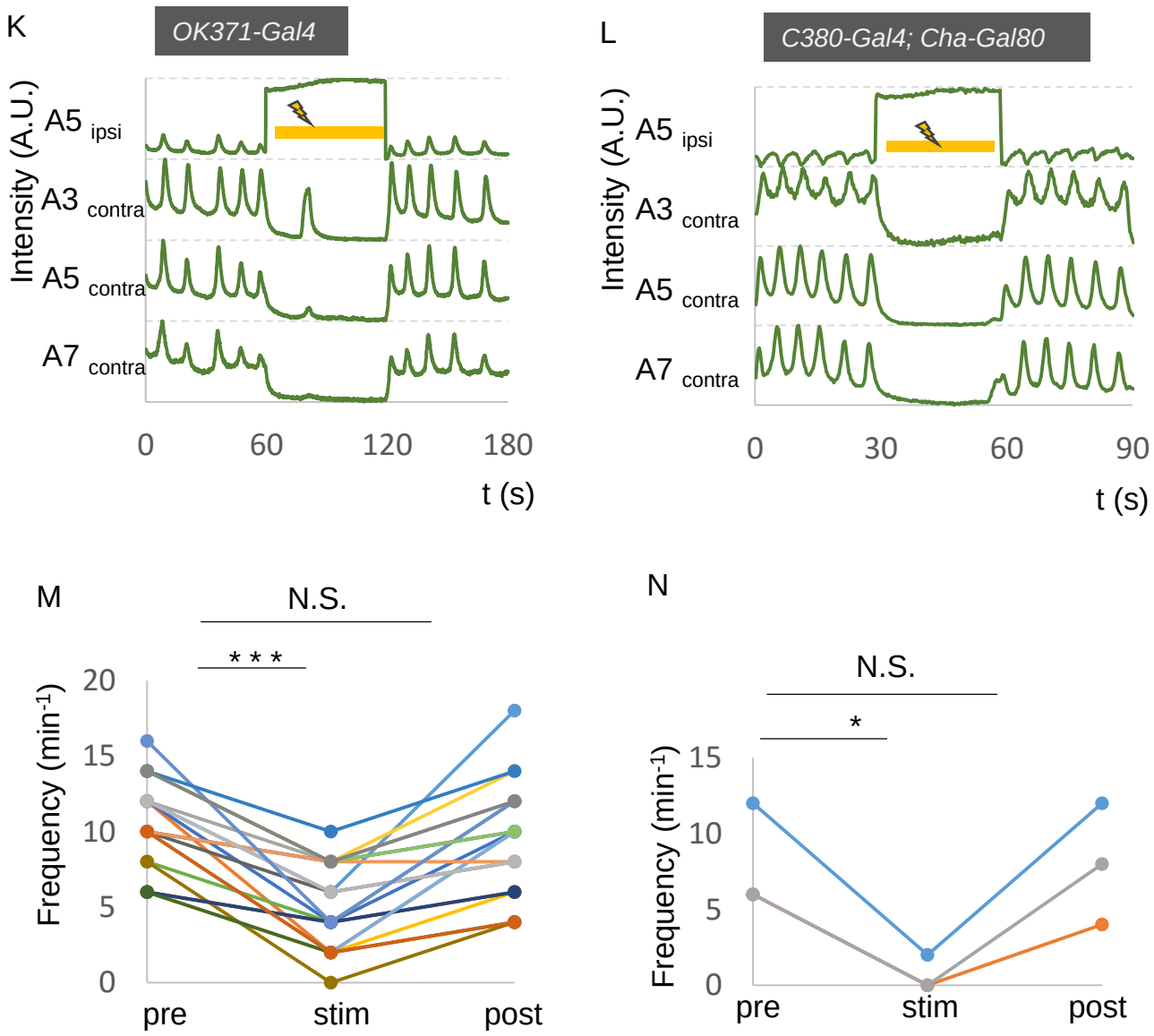

Fig. 3.3 Segment specific photo-inhibition of MNs in A5 decreased frequency of forward calcium wave dramatically.
(K, L) Representative result of GCaMP imaging with optogenetic inhibition by NpHR3 in A5 MNs is shown in expression of GCaMP6m and NpHR3::mcherry in (K) *OK371-Gal4*, (L) *C380-Gal4*; *Cha-Gal80* neurons. Yellow bar indicates yellow light stimulation. Fluorescence intensity in A3 contra, A5 ipsi and contra, and A7 contra nerve root each was plotted. (M, N) Frequency of forward calcium wave, before, during, and after A5 photo-stimulation was applied in (M) *OK371-Gal4* line, (N) in *C380-Gal4*; *Cha-Gal80* line. *P<0.05, ***P<0.001

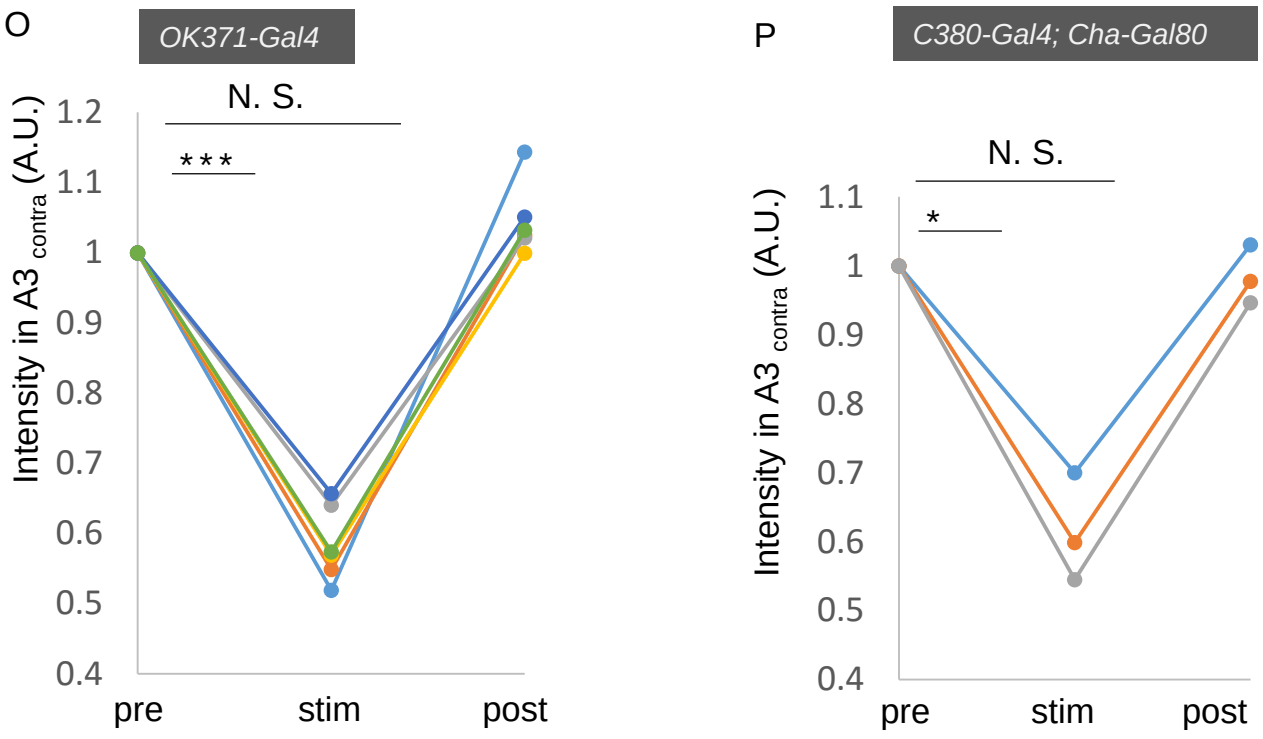

Fig. 3.3 Segment specific photo-inhibition of MNs in A5 decreased frequency of forward calcium wave dramatically.
(O, P) Fluorescent intensity in A3 ipsi in (O) *OK371-Gal4* neurons, (P) *C380-Gal4*; *Cha-Gal80* neurons before, during, and after A5 photo-stimulation was applied. *P<0.05, ***P<0.001

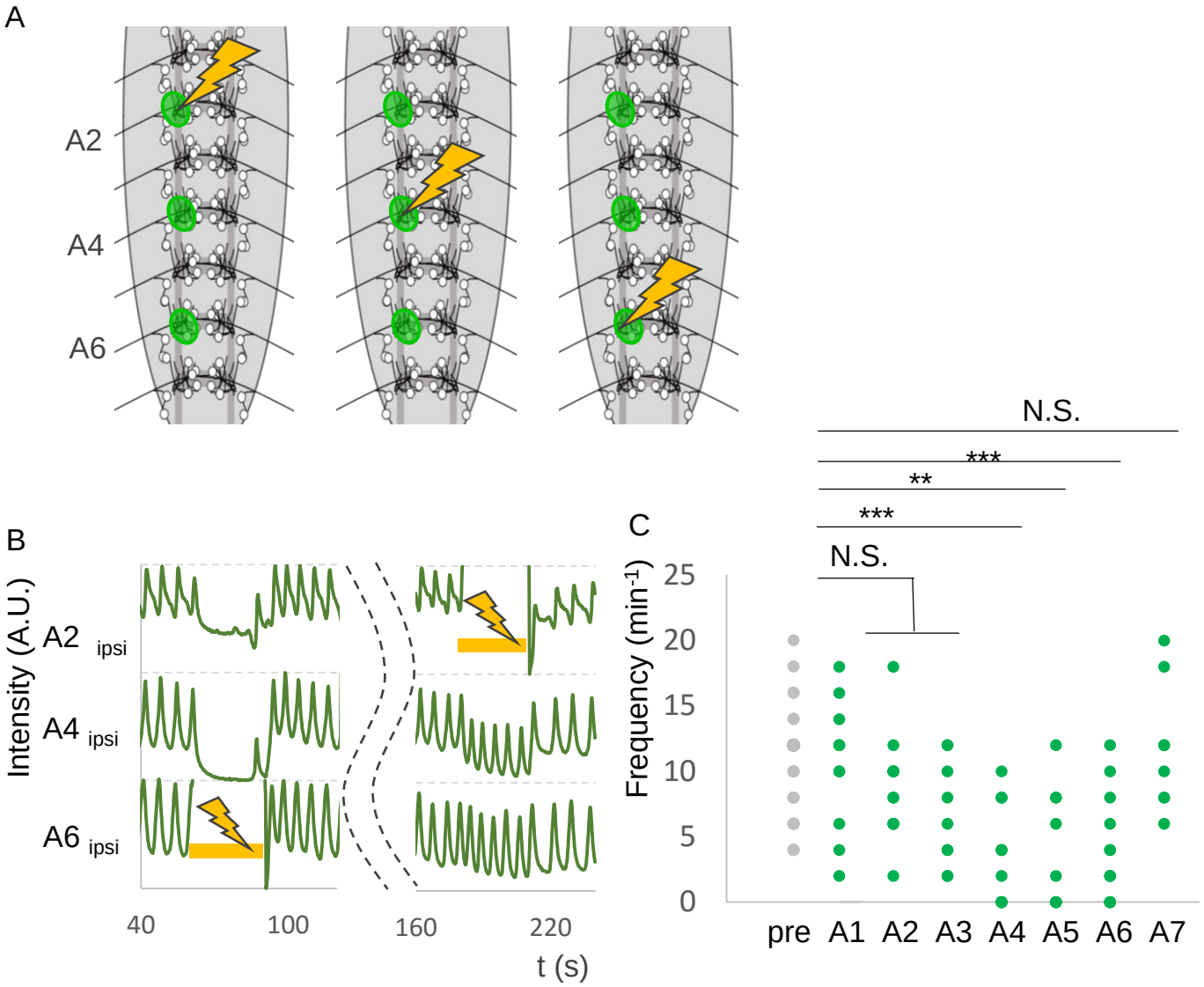

Fig. 3.4. Photo-inhibition of MNs in hemi-segment specific manner revealed inhibition of MNs activity around middle segment suppressed the forward calcium wave.

(A) Schematic of photo-inhibition application in hemi-segment specific manner in each neuromere. (B) Representative result of GCaMP imaging with optogenetic inhibition by NpHR3 in MNs is shown in expression of GCaMP6m and NpHR3::mcherry in *OK6-Gal4* neurons. Yellow bar indicates yellow light stimulation. Fluorescence intensity in A2 ipsi, A4 ipsi, and A6 ipsi nerve root each was plotted. (C) Frequency of forward calcium wave, pre stim, and during stim of A1, A2, A3, A4, A5, A6, and A7 applied. **P<0.01 , ***P<0.001

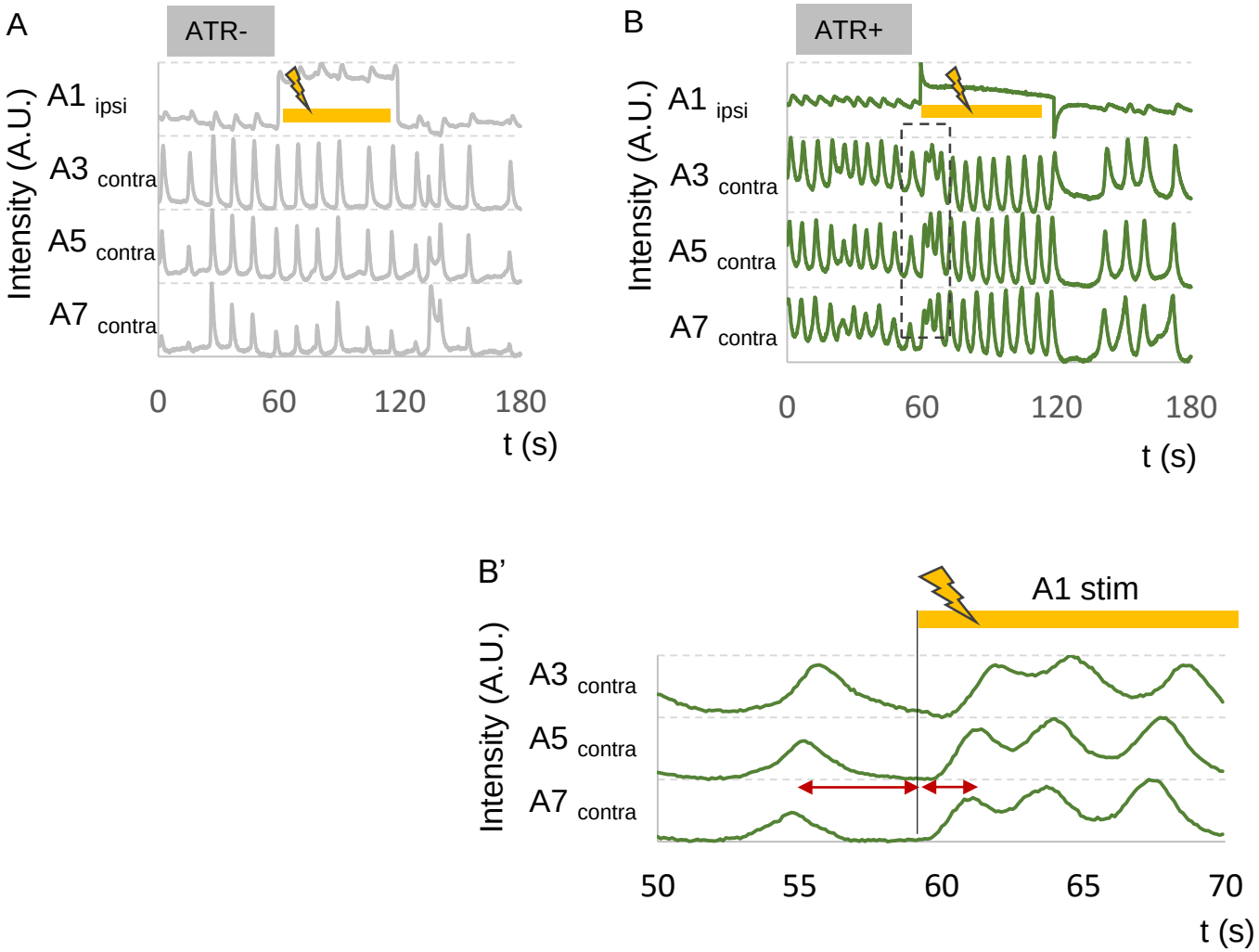

Fig. 3.5 Photo-inhibition of MNs in hemi-segment specific manner revealed inhibition of MNs activity in A1 segment induce the next forward calcium wave. (A, B) Representative result of GCaMP imaging with optogenetic inhibition in A1 MNs is shown in expression of GCaMP6m and NpHR3::mcherry in (A) *OK6-Gal4* neurons in ATR- control, (B) ATR+ experimental group. Yellow bar indicates yellow light stimulation. Fluorescence intensity in A1 ipsi, A3 contra, A5 contra, and A7 contra nerve root each was plotted. (B') Zoomed up image of (B) from 50 seconds to 70 seconds. Length of red lines are defined as "Latency", which are the time difference between A7 peak and the onset of photo-inhibition.

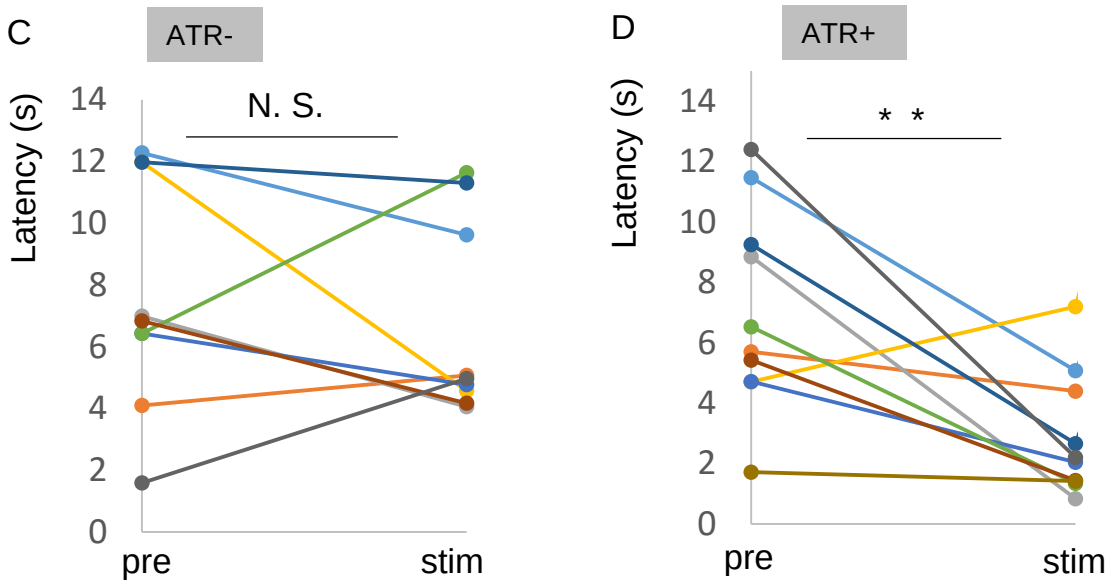

Fig. 3.5 Photo-inhibition of MNs in hemi-segment specific manner revealed inhibition of MNs activity in A1 segment induce the next forward calcium wave.
(C, D) “Latency” pre stim, and during stim A1 hemi-segment in (C) ATR- control, (D) ATR+ experimental group.

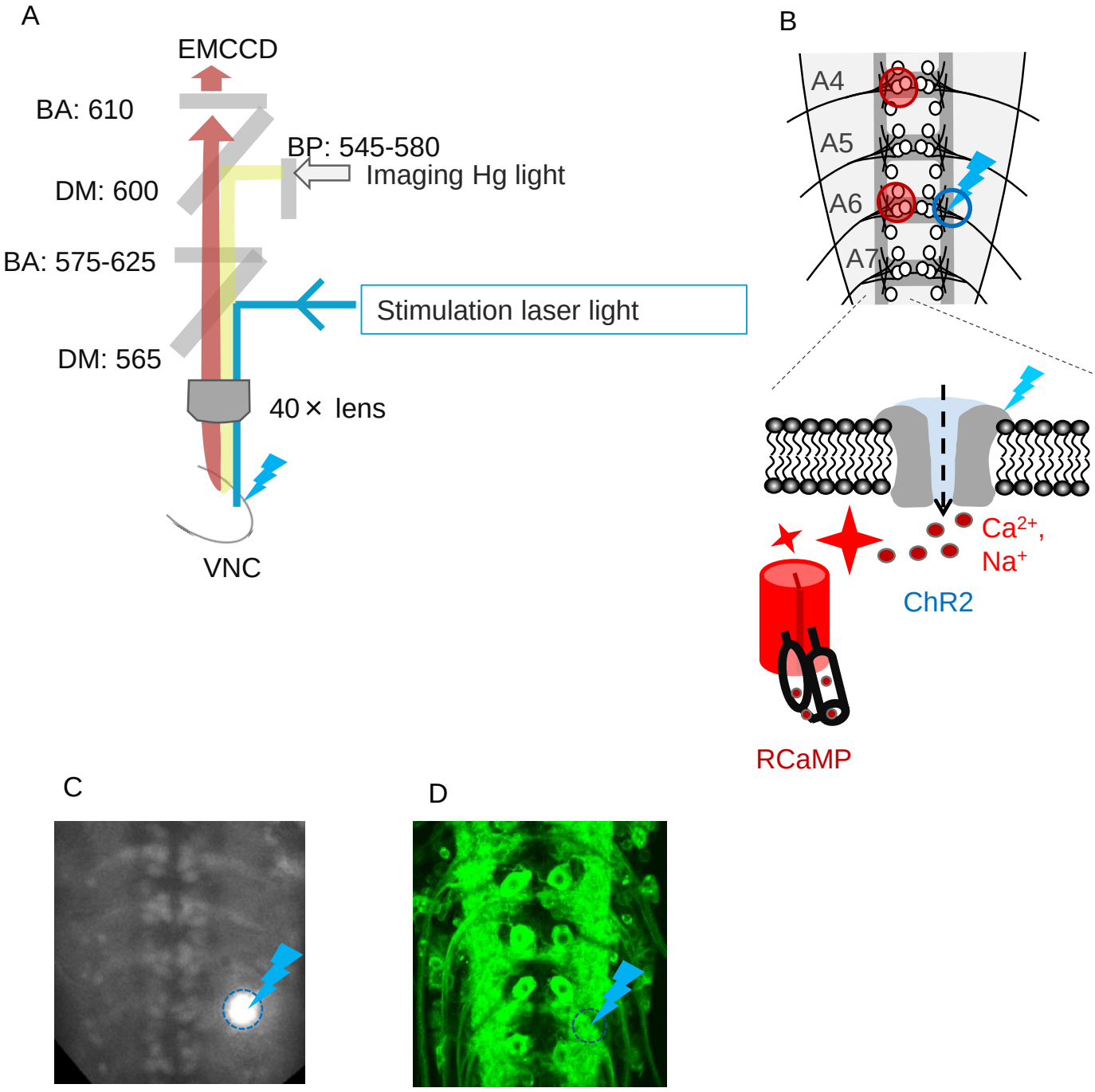

Fig. 3.6 Experimental system of simultaneous application of local photo-activation and calcium imaging.
(A) Schematic of simultaneous application of photo-activation and RCaMP imaging. BA; barrier filter, DM; dichroic mirror, BP; band pass filter. (B) Schematic of site of manipulation. Photo-activation of MNs was applied in blue circle. Red circles indicate a region of interest. (C) Single frame from RCaMP imaging of *OK6-Gal4* neurons when blue light was applied. (D) Expression pattern of the ChR2 (T159C)::YFP in *OK6-Gal4* line was assessed. Green represents YFP expression. Photo-activation of MNs was applied in blue circle.

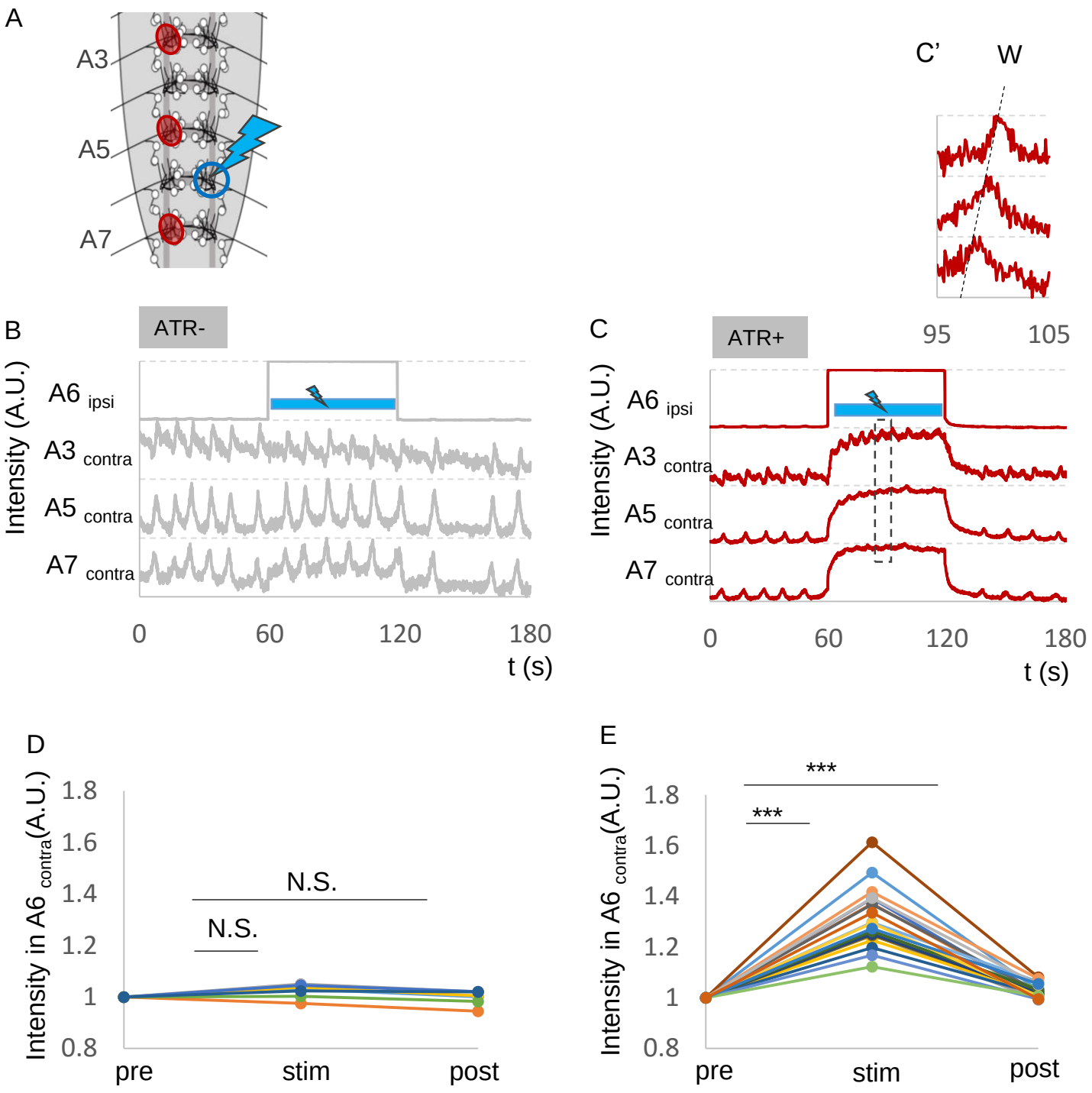

Fig. 3.7 Segment specific photo-activation of MNs in A6 increased frequency of forward calcium wave.

(A) Schematic of photo-activation application in A6 hemi-segment specifically.
(B, C) Representative result of RCaMP imaging with optogenetic activation by ChR2 in A6 MNs is shown in expression of RCaMP and ChR2(T159C)::YFP in *OK6-Gal4* neurons in (B) ATR- control, (C) ATR+ experimental group. Blue bar indicates blue light stimulation. Fluorescence intensity in A3 contra, A5 ipsi and contra, and A7 contra nerve root each was plotted. (C') Zoomed up image in (C) from 95 frame to 110 second. Broken black bar represents forward calcium wave. (D, E) Intensity in A6 contra, before, during, and after A6 photo-stimulation was applied to (D) ATR- control, (E) ATR+ experimental group.
***P<0.001

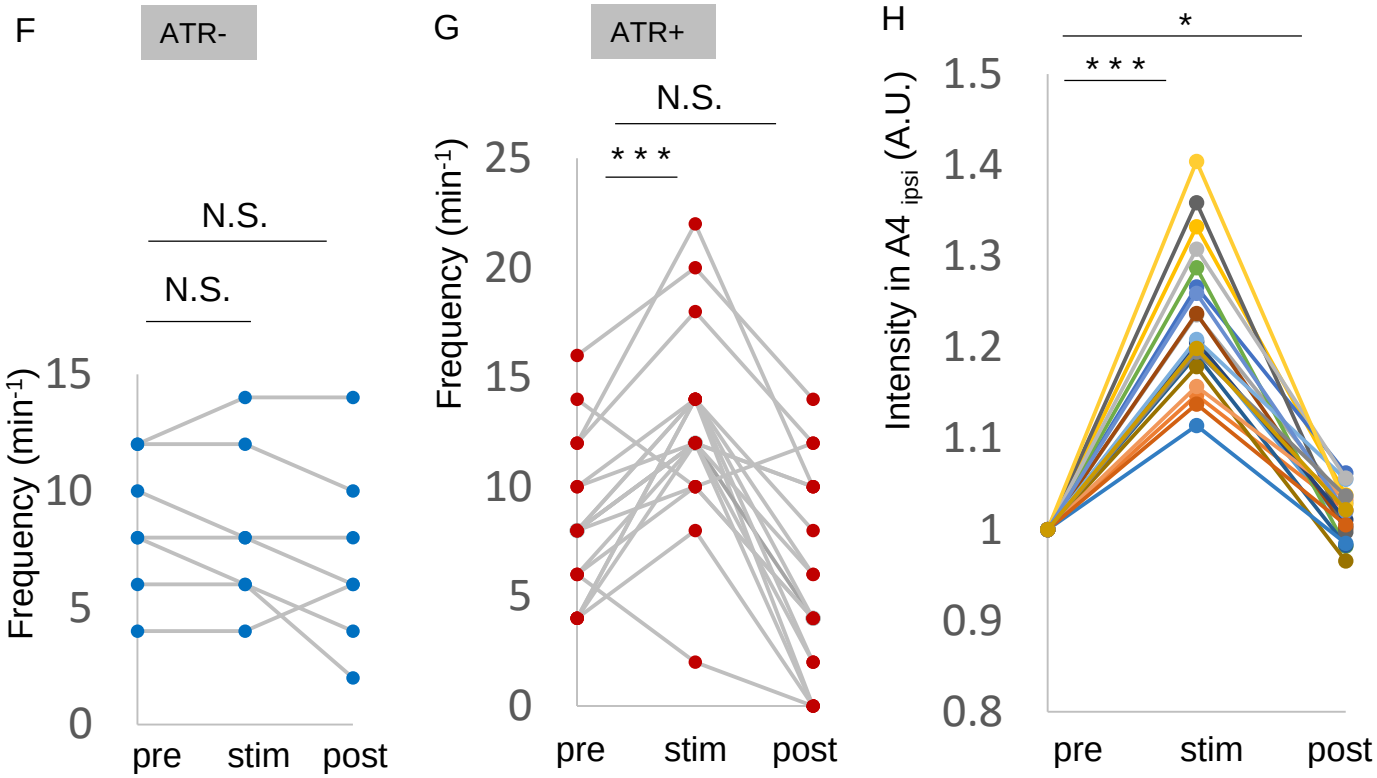

Fig. 3.7 Segment specific photo-activation of MNs in A6 increased frequency of forward calcium wave.
(F, G) Frequency of forward calcium wave, before, during, and after A6 photo-stimulation was applied to (F) ATR- control, (G) ATR+ experimental group. (H) Intensity in A4 ipsi, before, during, and after A6 photo-stimulation was applied. *P<0.05, ***P<0.001

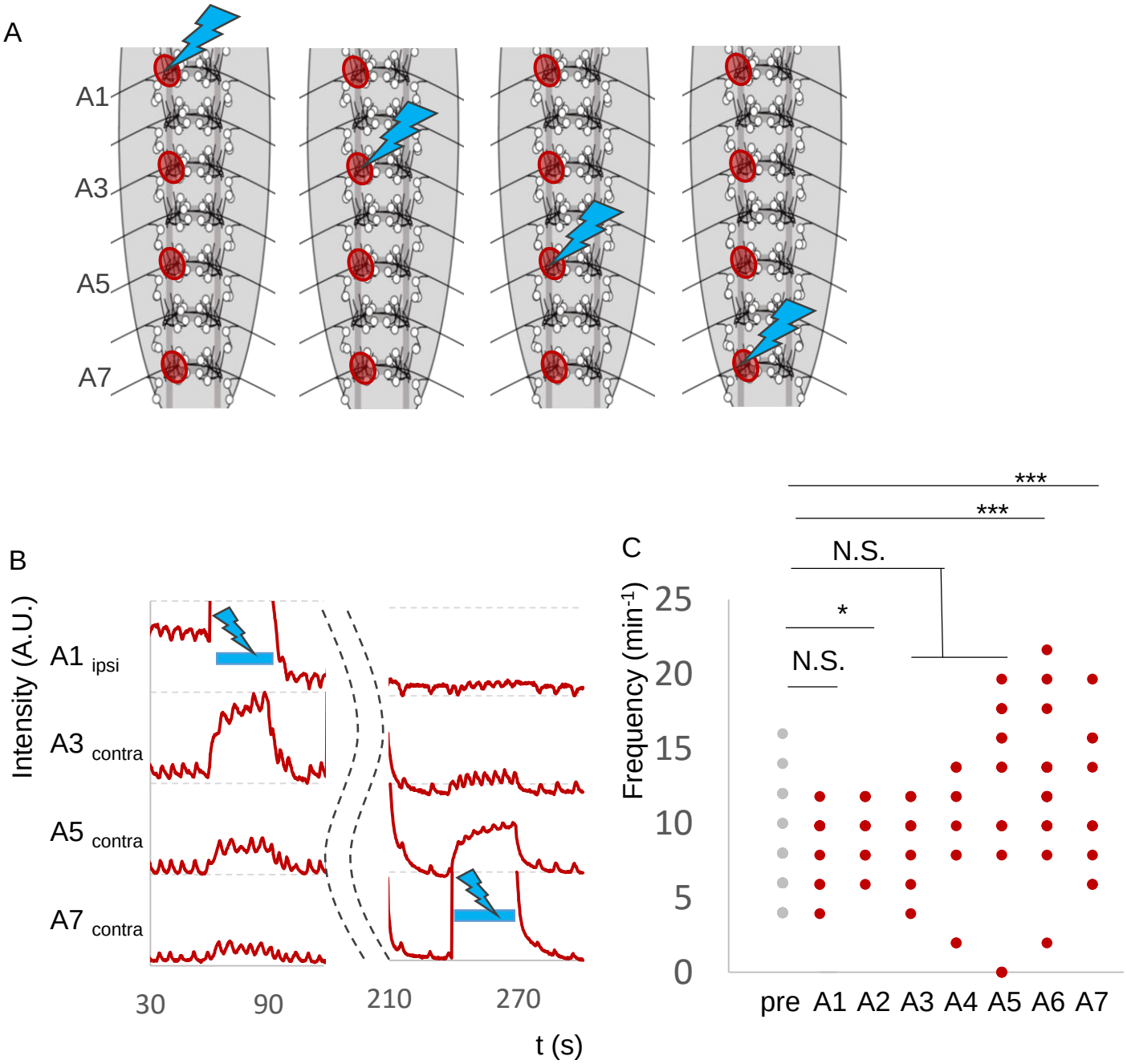

Fig. 3.8 Photo-activation of MNs in hemi-segment specific manner revealed photo-activation of MNs around posterior segment increased frequency of forward calcium wave.

(A) Schematic of photo-activation application in hemi-segment specific manner in each neuromere. (B) Representative result of RCaMP imaging with optogenetic activation by ChR2 in MNs is shown in expression of RCaMP and ChR2(T159C)::YFP in *OK6-Gal4* neurons. Blue bar indicates blue light stimulation. Fluorescence intensity in A1 contra, A3 contra, A5 ipsi and contra, A7 contra nerve root each was plotted. (C) Frequency of forward calcium wave, pre stim, during stim in A1, A2, A3, A4, A5, A6, and A7. *P<0.05 , ***P<0.001

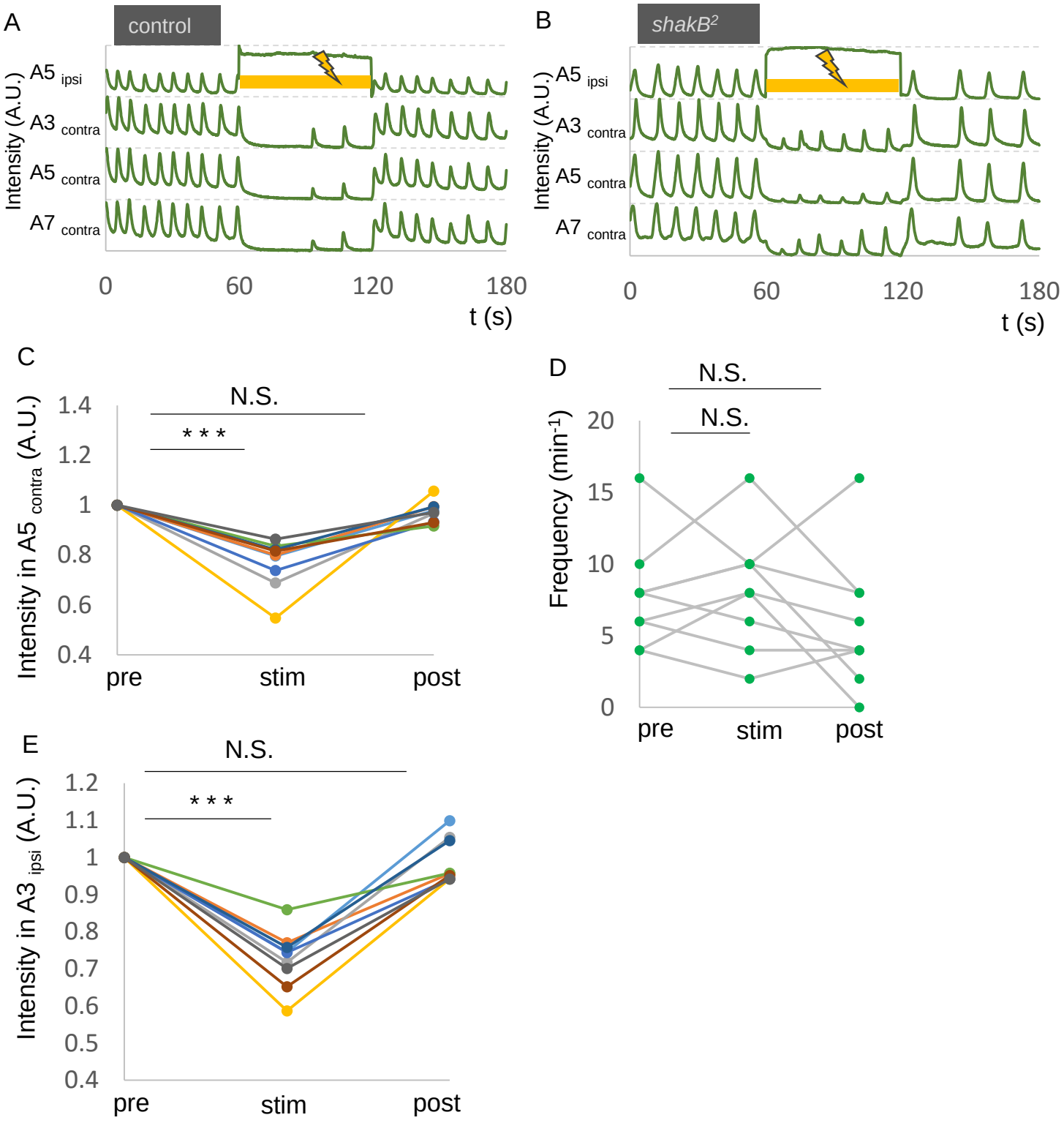

Fig. 3.9 Photo-inhibition in *shakB*^{2} mutant did not affect frequency of motor waves significantly.

(A, B) Representative result of GCaMP imaging with optogenetic inhibition by NpHR3 in MNs is shown in expression of GCaMP6m and NpHR3::mcherry in *OK6-Gal4* neurons in (A) control, (B) *shakB*^{2} mutant. Yellow bar indicates yellow light stimulation. Fluorescent intensity in A3 contra, A5 ipsi and contra, A7 contra nerve root each was plotted. (C) Intensity in A5 contra before, during, and after A5 photo-stimulation was applied. (D) Frequency of forward calcium wave before, during and after A5 photo-stimulation was applied. (E) Intensity in A3 ipsi, before, during, and after A5 photo-stimulation was applied. ***P<0.001

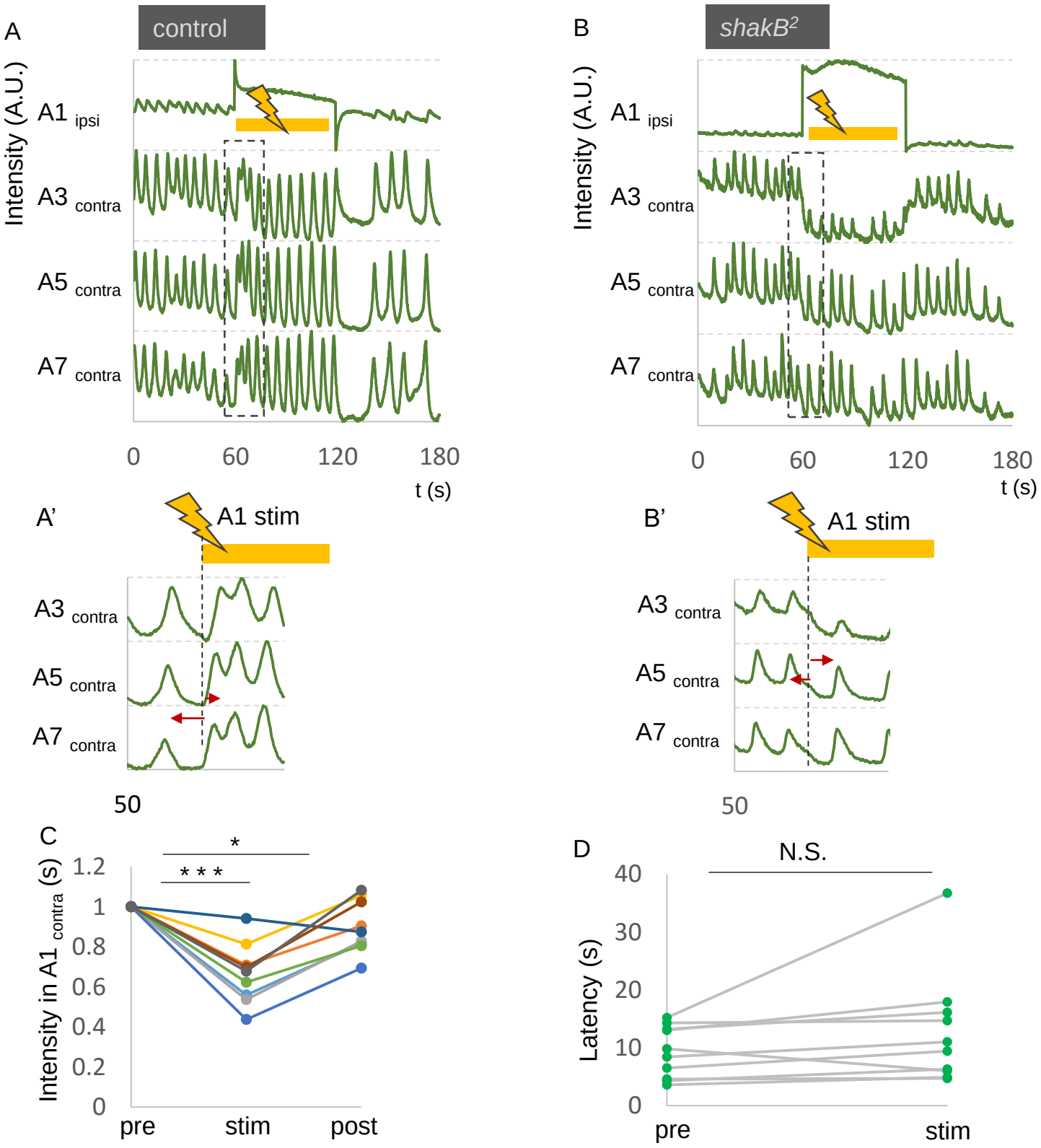

Fig. 3.10 Photo-inhibition in A1 in *shakB²* mutant did not induce motor wave.
(A, B) Representative result of GCaMP imaging with optogenetic inhibition by NpHR3 in A1 MNs is shown in expression of GCaMP6m and NpHR3::mcherry in *OK6-Gal4* neurons in (A) control, (B) *shakB²* mutant. Yellow bar indicates yellow light stimulation. Fluorescent intensity in A3 contra, A5 ipsi and contra, A7 contra nerve root each was plotted. (A', B') Zoomed up image of (A), and (B) from 50 seconds to 70 seconds respectively. Broken black bar indicates forward calcium wave. Length of red lines are defined as "Latency". (B) Intensity of A1 in contra before, during and after A5 photo-stimulation was applied. (C) Latency, before and during A1 photo-stimulation was applied. *P<0.05, ***P<0.001

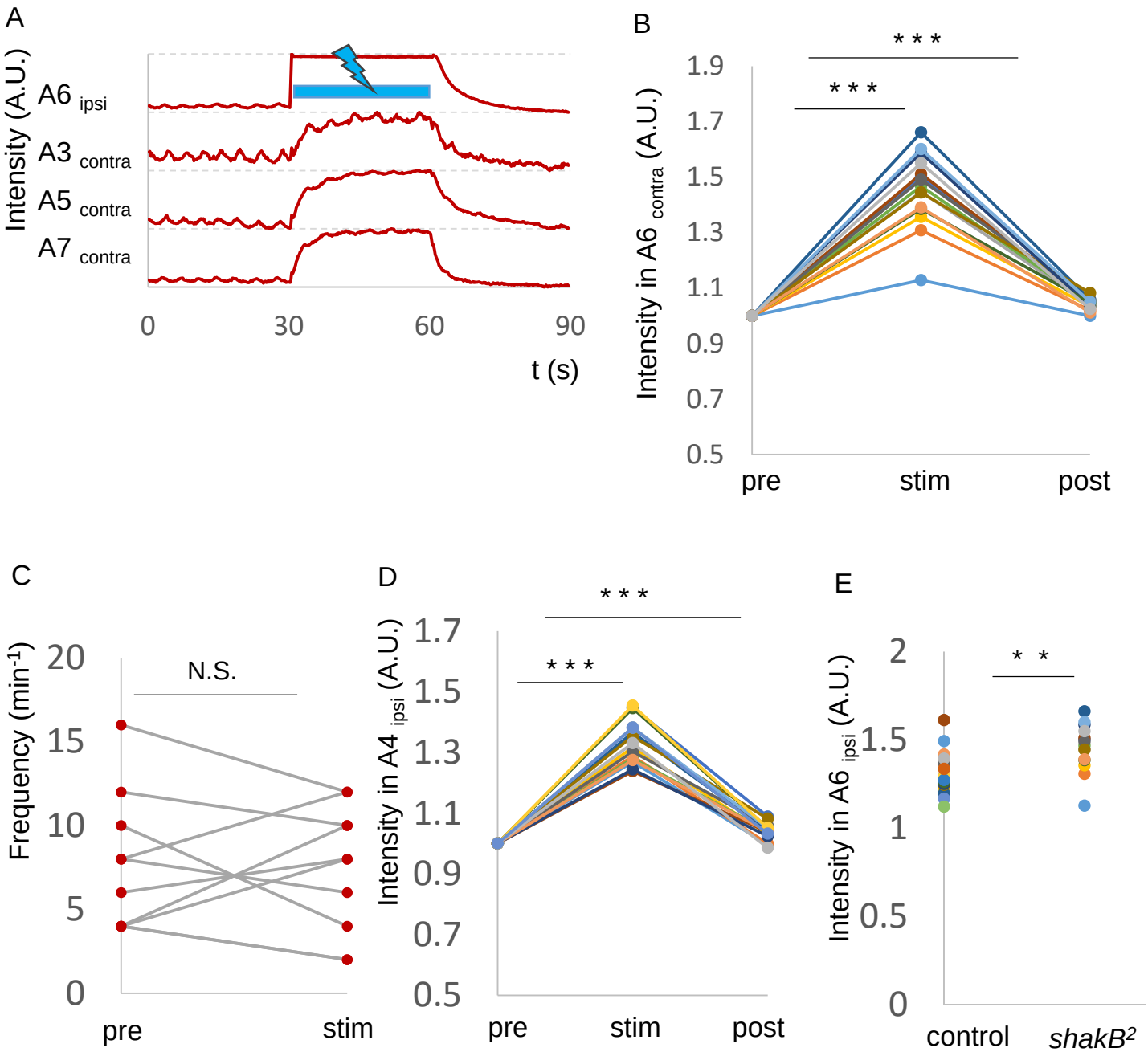

Fig. 3.11 Photo-activation in *shakB²* mutant did not affect frequency of forward calcium wave significantly.

(A) Representative result of RCaMP imaging with optogenetic activation by ChR2 in A6 MNs is shown in expression of RCaMP and ChR2(T159C)::YFP in *OK6-Gal4* neurons in *shakB²* mutant. Blue bar indicates blue light stimulation. Fluorescent intensity in A3 contra, A5 ipsi and contra, A7 contra nerve root each was plotted. (B) Intensity in A6 contra before, during, and after A5 photo-stimulation was applied. (C) Frequency of forward calcium wave before, during and after A6 photo-stimulation was applied. (D) Intensity in A4 ipsi, before, during, and after A6 photo-stimulation was applied. (E) Intensity in A6 contra during A6 photo-stimulation in control, and *shakB²* mutant

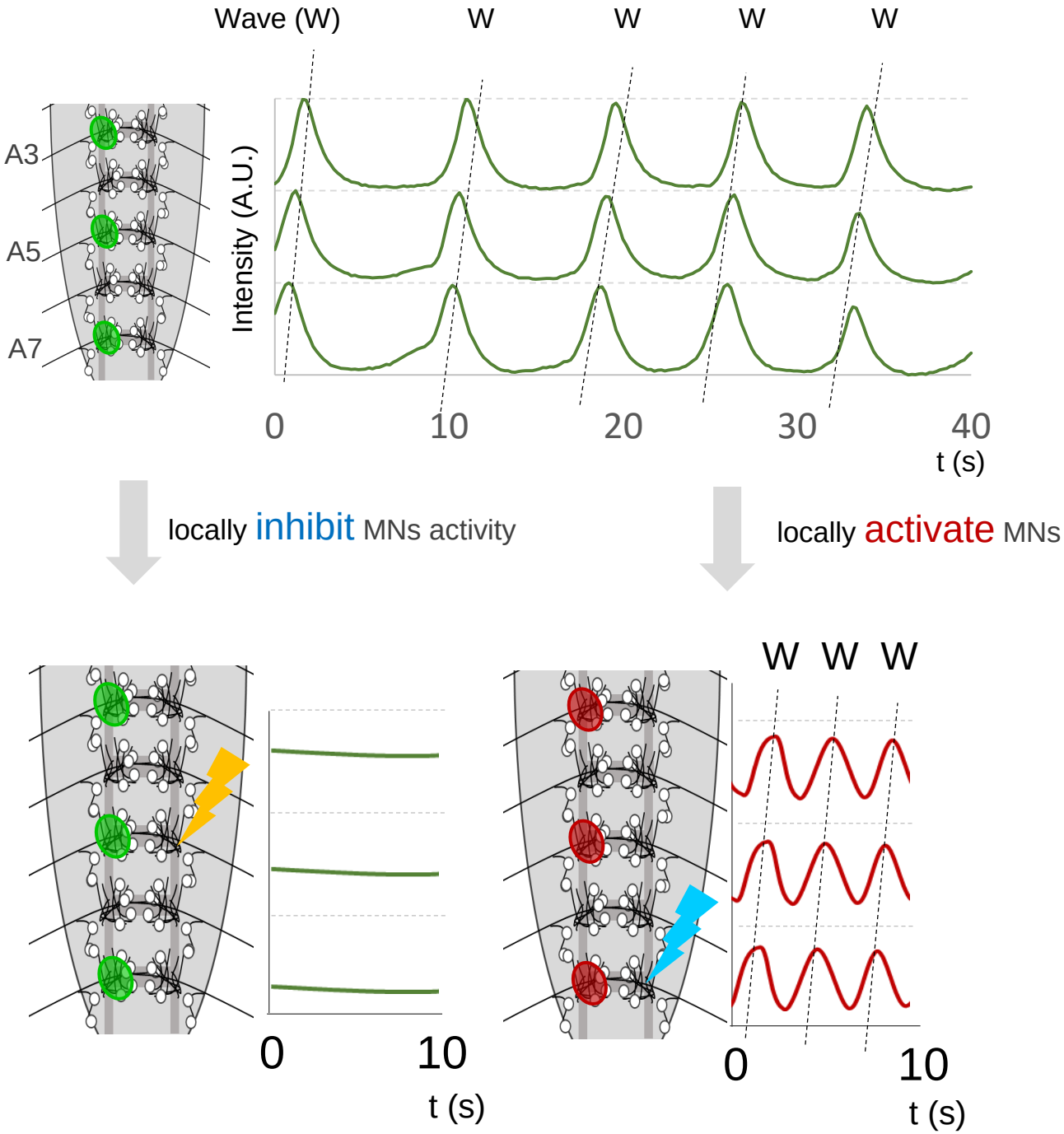

Fig. 4.1 Summary of segment specific manipulation of motoneruons
Segment specific photo-inhibition of MNs in around middle segments (A4, A5, A6) decreased the frequency of forward calcium wave (lower left). Segment specific photo-activation of MNs in posterior segments (A6, A7) increased the frequency of forward calcium wave (lower right).

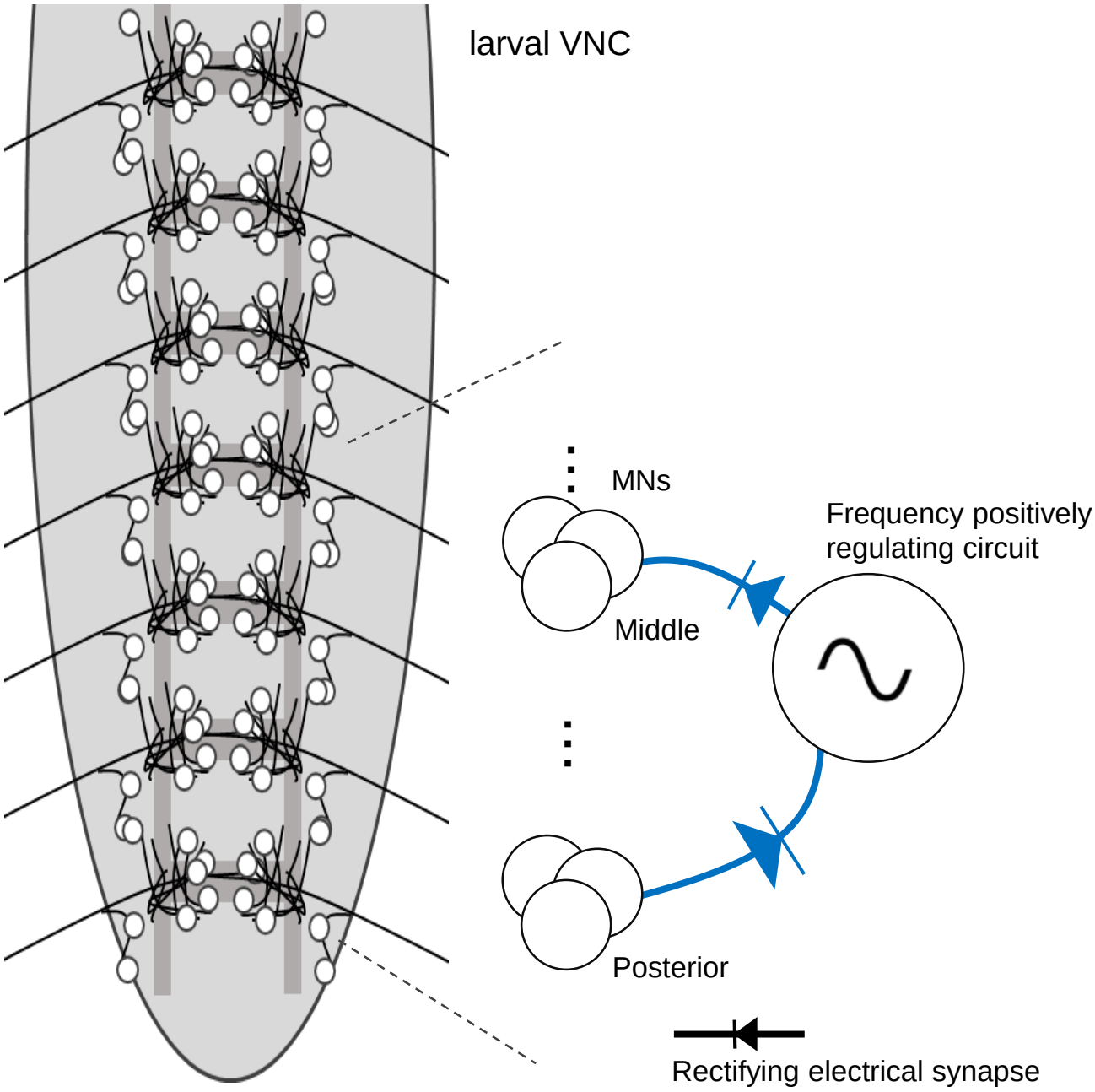

Fig. 4.2 Model of the frequency modulation via motoneuronal rectifying electrical synapses
In middle segments, MNs may be connected to the neurons which are involved in the regulation of the wave frequency via negatively rectifying electrical synapses. This will allow anion flow from MNs to the regulator neurons upon photo-inhibition of MNs, which in turn will result in a decrease in the frequency, while preventing cation flow upon photo-activation of MNs. In contrast, in posterior segments, MNs may couple to the regulator neurons via positively rectifying electrical synapses. This would allow cation flow from MNs to the regulator neurons upon photo-activation of MNs, which in turn increases the wave frequency, while preventing anion flow between the neurons upon photo-inhibition of MNs.

7. Acknowledgements

I would like to express my sincere gratitude to my advisors Dr. Akinao Nose and Dr. Hiroshi Kohsaka for their invaluable, constant encouragement and support. I am grateful to Dr. Etsuko Takasu-Ishikawa for constructive comments and warm encouragement.

I would like to thank all the past and the present members of the Nose lab, especially, Dr. Eri Hasegawa, Dr. Kaoru Masuyama, Dr. Yuki Itakura, Dr. Satoko Okusawa, Dr. Akira Fushiki, Mr. Kengo Inada, Mr. Takafumi Sawai, Mr. Shunsuke Takagi, Mr. Koichi Teranishi, Mr. Tappei Kawasaki, Mr. Keisuke Ban, Mr. Ryota Mori, Mr. Youngtaek Yoon, Mr. Dojin Miyamoto, Mr. Yoshiki Maruta, Ms. Yumi Sakamaki, Mr. Suguru Takagi, Mr. Hitoshi Maruo, Mr. Yasuhide Lee, Mr. Jeonghyuk Park, Ms. Maki Kusano, Mr. Tatsuya Takatori, and Mr. Atsuki Hiramoto. I am also thankful to Ms. Sawako Niki, Ms. Toshie Naoi, and Ms. Kasumi Shiabahara for technical and administrative supports.

I am thankful to the members of my thesis committee: Dr. Masato Okada, Dr. Tetsuya Kojima, Dr. Tomoki Fukai, and Dr. Tatsuhiro Hisatsune.